Bioactive Materials 22 (2023) 326–342

Contents lists available at ScienceDirect

Bioactive Materials

journal homepage: www.keaipublishing.com/en/journals/bioactive-materials

Small extracellular vesicles derived from hypoxic preconditioned dental pulp stem cells ameliorate inflammatory osteolysis by modulating macrophage polarization and osteoclastogenesis

Jun Tian [a,b,1], Weiyang Chen [a,b,1], Yuhua Xiong [a,b,1], Qianer Li [a,b], Siyi Kong [a,b], Mengjie Li [a,b], Chunfeng Pang [a,b], Yu Qiu [a,b], Zhezhen Xu [a,b], Qimei Gong [a,b,*], Xi Wei [a,b,**]

[a] Hospital of Stomatology, Guanghua School of Stomatology, Sun Yat-Sen University, Guangzhou, Guangdong, 510055, PR China
[b] Guangdong Provincial Key Laboratory of Stomatology, Guangzhou, Guangdong, 510055, PR China

ARTICLE INFO

Keywords:
Dental pulp stem cells
Small extracellular vesicles
Macrophage
Osteoclast
Inflammatory osteolysis

ABSTRACT

Extensive macrophage inflammatory responses and osteoclast formation are predominant during inflammatory or infective osteolysis. Mesenchymal stem cell (MSC)-derived small extracellular vesicles (MSC-sEV) have been shown to exert therapeutic effects on bone defects. However, cultured MSCs are typically exposed to normoxia (21% O_2) *in vitro*, which differs largely from the oxygen concentration *in vivo* under hypoxic conditions. It is largely unknown whether sEV derived from dental pulp stem cells (DPSCs) cultured under hypoxic conditions (Hypo-sEV) exert better therapeutic effects on lipopolysaccharide (LPS)-induced inflammatory osteolysis than those cultured under normoxic conditions (Nor-sEV) by simultaneously inhibiting the macrophage inflammatory response and osteoclastogenesis. In this study, we show that hypoxia significantly induces the release of sEV from DPSCs. Moreover, Hypo-sEV exhibit significantly improved efficacy in promoting M2 macrophage polarization and suppressing osteoclast formation to alleviate LPS-induced inflammatory calvarial bone loss compared with Nor-sEV. Mechanistically, hypoxia preconditioning markedly alters the miRNA profiles of DPSC-sEV. MiR-210-3p is enriched in Hypo-sEV, and can simultaneously induce M2 macrophage generation and inhibit osteoclastogenesis by targeting *NF-κB1 p105*, which attenuates osteolysis. Our study suggests a promising potential for hypoxia-induced DPSC-sEV to treat inflammatory or infective osteolysis and identifies a novel role of miR-210-3p in concurrently hindering osteoclastogenesis and macrophage inflammatory response by inhibiting *NF-kB1* expression.

1. Introduction

A healthy microenvironment around bone tissue is critical for maintaining bone homeostasis. In bone-related inflammatory diseases, including osteomyelitis, periodontitis, peri-implantitis, rheumatoid arthritis (RA) and septic arthritis, key innate immune cells, such as macrophages, are recruited and polarized to the M1 proinflammatory phenotype [1,2]. These M1 macrophages with prolonged activity subsequently produce high levels of nitric oxide (NO), reactive oxygen species and proinflammatory cytokines, such as IL-1β, IL-6 and TNF-α, leading to a sustained inflammatory response. Proinflammatory cytokines can promote receptor activator of NF kappa B ligand (RANKL) production in osteoblasts or other resident cells, such as periodontal ligament cells, leading to excessive osteoclast formation and activity, bone resorption and the disequilibrium of bone homeostasis [3]. Given the critical role of proinflammatory M1 macrophages and excessive osteoclastogenesis in bone destruction, inhibiting macrophage inflammatory responses or inducing macrophages to differentiate into the anti-inflammatory M2 phenotype, as well as inhibiting osteoclast formation, have been considered promising strategies to treat

Peer review under responsibility of KeAi Communications Co., Ltd.
* Corresponding author. Hospital of Stomatology, Guanghua School of Stomatology, Sun Yat-Sen University, 56 Ling Yuan Xi Road, Guangzhou, 510055, China.
** Corresponding author. Hospital of Stomatology, Guanghua School of Stomatology, Sun Yat-Sen University, 56 Ling Yuan Xi Road, Guangzhou, 510055, China.
E-mail addresses: tianjun2@mail2.sysu.edu.cn (J. Tian), chenwy27@mail2.sysu.edu.cn (W. Chen), xiongyh8@mail2.sysu.edu.cn (Y. Xiong), gongqim@mail.sysu.edu.cn (Q. Gong), weixi@mail.sysu.edu.cn (X. Wei).
[1] Jun Tian, Weiyang Chen and Yuhua Xiong contributed equally to this study.

https://doi.org/10.1016/j.bioactmat.2022.10.001
Received 19 August 2022; Received in revised form 23 September 2022; Accepted 1 October 2022
2452-199X/© 2022 The Authors. Publishing services by Elsevier B.V. on behalf of KeAi Communications Co. Ltd. This is an open access article under the CC BY-NC-ND license (http://creativecommons.org/licenses/by-nc-nd/4.0/).

inflammatory bone resorption [4]. Current antiresorptive drugs, including bisphosphonate, cathepsin K inhibitors and RANKL inhibitors (such as denosumab), can effectively inhibit bone resorption, but these agents have numerous side effects, including renal toxicity, high-allergic reactions and osteonecrosis of the jaw [5]. Furthermore, these drugs do not exert immunomodulatory effects to induce M2 macrophage generation and ameliorate the inflammatory response. Thus, it is crucial to exploit novel therapeutic methods for the remedy and prophylaxis of inflammatory osteolysis.

Mesenchymal stem cells (MSCs) are adult fibroblast-like pluripotent cells with the capacity for self-renewal and multipotent differentiation. Due to their powerful immunomodulatory capacities, MSCs have been widely used to treat diverse inflammatory diseases, including bone-related inflammatory diseases such as RA and periodontitis [6–8]. Increasing evidence has demonstrated that the therapeutic effects of MSCs are primarily attributed to their secretory paracrine factors, the most crucial of which are extracellular vesicles (EVs), including exosomes. Small extracellular vesicles (sEV), which range from 30 nm to 200 nm in size, are lipid EVs produced by the fusion of multivesicular bodies with the cellular membrane and contain RNA, DNA, lipids and proteins. By transmitting extrinsic miRNAs and other molecular signals, sEV play an important role in intercellular communication. MSC-sEV show therapeutic effects, including immunoregulation and the induction of tissue repair or regeneration, similar to those of their parent MSCs. Furthermore, sEV derived from MSCs have advantages over MSC therapy regarding efficacy, safety, storage and administration [9–12]. Numerous studies have revealed that MSC-sEV induce M2 macrophage polarization to facilitate bone repair in bone defect and inflammatory osteolysis models, such as RA and periodontitis [13–16]. Moreover, several recent studies reported that MSC-sEV directly inhibited osteoclast differentiation to ameliorate bone resorption in ovariectomy (OVX) and hindlimb unloading-induced osteoporosis [11,17]. Therefore, the administration of MSC-sEV is considered as a highly promising cell-free approach to treat bone-related inflammatory diseases.

Dental pulp stem cells (DPSCs) are MSCs isolated from adult dental pulp. DPSCs can be easily obtained from extracted teeth with minimal invasiveness, raising no ethical concerns [18]. Compared with classic bone marrow MSCs (BMSCs), DPSCs exhibit a higher proliferation rate [19]. In addition, DPSC-sEV were reported to show stronger immunoregulatory effects than BMSC-sEV [20]. Therefore, DPSC-sEV may be acquired more conveniently with higher production and bioactivities than BMSC-sEV. DPSC-sEV have also been documented to exert therapeutic effects on skin wounds, spinal cord injury, and mandible and calvarial bone defects [18,21–24]. However, it is largely unknown whether DPSC-sEV can simultaneously directly suppress the macrophage inflammatory response and osteoclastogenesis to induce bone repair in inflammatory osteolysis.

The compositions of MSC-sEV control their therapeutic effects but vary profoundly depending on the cellular microenvironment. Hypoxia helps maintain MSC properties, including proliferation, differentiation, and self-renewal, while enhancing the biological activities of sEV derived from MSCs [25]. However, MSCs that are cultured or expanded *in vitro* are typically exposed to normoxia (21% O_2), which is different from the oxygen concentration found in the body under natural physiological conditions. In fact, a large proportion of MSCs *in vivo* exist in a hypoxic environment with oxygen concentrations ranging from 2% to 8% or even lower [24]. Our previous study indicated that the proteomics of hypoxia-preconditioned DPSC-derived sEV were significantly different from those of control DPSC-sEV. More importantly, hypoxia-preconditioned DPSC-derived sEV showed increased angiogenic potential [26]. However, whether DPSC-sEV produced under hypoxic conditions exert better therapeutic effects on inflammatory osteolysis by inhibiting the macrophage inflammatory response and osteoclastogenesis remains largely unknown. In this study, we show that hypoxic DPSC-sEV alleviate lipopolysaccharide (LPS)-induced inflammatory bone loss by transferring miR-210-3p, which directly targets NF-κB1 to inhibit both the macrophage inflammatory response and osteoclast formation.

2. Materials and methods

2.1. Animals

Five-week-old Sprague–Dawley (SD) rats and eight-to ten-week-old C57/BL6 male mice were obtained from the Laboratory Animal Center of Sun Yat-Sen University. All animal experiments were approved by the Institutional Animal Care and Use Committee of Sun Yat-Sen University (No. SYSU-IACUC-2022-000089).

2.2. Isolation and culture of DPSCs

DPSCs were isolated from pulpal tissues in the maxillary central incisors of SD rats. After extracting the maxillary central incisors of SD rats with surgical scissors and removing partial enamel and dentin with forceps, pulp tissues were isolated and rinsed in α-minimum essential medium (α-MEM, Gibco; Thermo Fisher Scientific, MA, USA) and sliced by ophthalmic scissors. Minced pulp tissues were cultured in α-MEM supplemented with 20% fetal bovine serum (FBS, Gibco, USA), 100 U/mL penicillin and 100 μg/mL streptomycin (Invitrogen, CA, USA) at 37 °C in a humidified chamber with 5% CO_2. The medium was changed every three days. DPSCs at passages 3–5 were used in the following experiments.

2.3. Characterization of DPSCs

2.3.1. Flow cytometric analysis of surface markers

The mesenchymal phenotype of DPSCs was determined by flow cytometric analysis. DPSCs in suspension were collected and stained with CD29-APC, CD44/CD90-PE, CD34-FITC, and CD45-PE (BD Bioscience, San Jose, CA, USA) monoclonal antibodies for 30 min at 4 °C. The expression profiles were analyzed with a flow cytometer (BD Bioscience, USA).

2.3.2. Identification of osteogenic and adipogenic capabilities of DPSCs

DPSCs were seeded in 6-well plates (Corning, USA) at 3×10^5 cells/well. To induce osteogenic or adipogenic differentiation of DPSCs, the culture medium was changed to osteogenic medium (OM) containing 2 mM β-glycerophosphate (Sigma–Aldrich, MO, USA), 100 μM L-ascorbic acid 2-phosphate (Sigma–Aldrich), and 10 nM dexamethasone (Sigma–Aldrich, USA) or commercial adipogenic medium (Cyagen Biosciences, Guangzhou, China), respectively. After 14 days of induction, the cells were washed with PBS, fixed in 4% paraformaldehyde (Biosharp, Hefei, China) for 30 min at room temperature, and subsequently subjected to Alizarin Red staining (ARS, Cyagen Biosciences, China) or Oil Red O staining (Cyagen Biosciences, China). Mineralized nodules and lipid droplets were observed and photographed.

2.3.3. Immunofluorescence staining of vimentin and cytokeratin

DPSCs were seeded in 24-well plates (Corning, NY, USA) at 5×10^4 cells/well. After 24 h, the cells were fixed with 4% paraformaldehyde (Biosharp, China) for 15 min, permeabilized with 0.1% Triton X-100 (Sigma–Aldrich, USA) for 15 min, and then blocked with 5% bovine serum albumin (BSA) for 30 min at room temperature. The cells were subsequently incubated with vimentin antibodies (Abcam, Cambridge, UK) at a 1:200 dilution and cytokeratin-14 antibodies (Affinity, Changzhou, China) at a 1:100 dilution overnight at 4 °C and then incubated with Alexa Fluor 488- and/or Alexa Fluor 594-conjugated secondary antibodies. To visualize the nuclei, the cells were stained with 4′,6-diamidino-2-phenylindole (DAPI; Abcam, UK).

2.4. Isolation, characterization and quantitation of sEV

The isolation of DPSC-sEV was performed according to the guidelines from the International Society for Extracellular Vesicles (MISEV2018). Briefly, 80–90% confluent DPSCs were rinsed with PBS and then cultured in serum-free medium for 48 h with 21% O_2 (normoxia) or 1% O_2 (hypoxia). The conditioned medium was collected and centrifuged sequentially at 800×*g* for 10 min and 3000×*g* for 10 min to remove cell debris and large vesicles and then ultracentrifuged at 100,000×*g* for 60 min at 4 °C (Beckman Coulter, Germany). After the supernatant was discarded, purified sEV derived from DPSCs under normoxic (Nor-sEV) or hypoxic (Hypo-sEV) conditions were resuspended in PBS and stored at −80 °C. The sEV proteins were quantified using the Pierce BCA Protein Assay (Thermo Fisher Scientific, MA, USA). The size distribution and ultrastructure of purified Nor-sEV and Hypo-sEV were determined using a NanoSight and transmission electron microscopy (TEM). Furthermore, the sEV-specific protein markers CD9, CD63 and TSG101 were analyzed by western blotting, and β-actin was used to quantify the amount of loaded protein.

2.5. Transmission electron microscopy (TEM)

A total of 10 μL of purified Nor-sEV or Hypo-sEV was placed on copper mesh and incubated at room temperature for 1 min. After being washed with sterile distilled water, the sEV-enriched fraction was contrasted by a uranyl acetate solution for 1 min. The sample was then dried for 2 min under incandescent light. The copper mesh was observed and photographed under a JEM-1400 electron microscope (JEOL Ltd., Japan).

2.6. Nanoparticle tracking analysis (NTA)

The size distribution and particle concentration of purified Nor-sEV and Hypo-sEV were determined using a NanoSight LM10 (NanoSight Ltd., Malvern, England) with constant flow injection. Particle movement (detection time: 5 × 30 s) was analyzed using NTA software (NTA 3.1).

2.7. Western blotting

Total protein was extracted from RAW264.7 cells, purified Nor-sEV and Hypo-sEV using RIPA lysis buffer with protease and phosphatase inhibitors (Thermo Fisher Scientific, USA). The protein concentration was quantified using a bicinchoninic acid protein assay kit (Thermo Fisher Scientific, USA). For Western blot analysis of cell lysates, 30 μg of protein was separated by SDS-polyacrylamide gel electrophoresis (SDS–PAGE; Invitrogen, USA) and transferred to PVDF membranes (Millipore, MA, USA). The membranes were blocked with 5% BSA (Sigma, USA) for 1 h at room temperature, followed by overnight incubation at 4 °C with the primary antibodies diluted in blocking solution according to the manufacturer's instructions. The following primary antibodies were used: mouse anti-CD9/63, mouse anti-TSG101 (Santa Cruz Biotechnology, CA, USA), rabbit anti-iNOS (Abcam, Cambridge, UK), rabbit anti-Arg1 (Cell Signaling Technology, MA, USA), mouse anti-NF-κB p105 and anti-p50 (Zen BioScience, Chengdu, China), and mouse anti-β-actin (Sigma–Aldrich, USA). The membranes were then incubated for 1 h at room temperature in species-related horseradish peroxidase (HRP)-conjugated secondary antibodies (1:10,000; Cell Signaling Technology, USA). The immunoreactive proteins were detected using a chemiluminescence kit (Millipore, USA).

2.8. LPS-induced in vivo calvarial osteolysis mouse model

The mouse calvarial osteolysis model induced by LPS (derived from *Escherichia coli* O111:B4; Sigma–Aldrich, MO, USA) was established as previously described [27]. Briefly, the mice received a subcutaneous injection of 25 mg/kg LPS over the sagittal midline suture of the calvarium under anesthesia. To evaluate the therapeutic effects of Nor-sEV and Hypo-sEV on LPS-induced calvarial osteolysis, 100 μg of Nor-sEV or Hypo-sEV per mouse was simultaneously injected with LPS. After 7 days, all mice were sacrificed. Then, the calvarial bones were collected and fixed in 4% paraformaldehyde for 24 h for further micro-CT and histological analysis.

2.9. Microcomputed tomography (micro-CT)

The calvaria bones were scanned using high-resolution micro-CT (μCT-50, SCANCO Medical AG). The scanning parameters were as follows: 70 kV, 114 μA, and 7 μm. The μCT Evaluation Program V6.6 (SCANCO, Switzerland) was used to generate three-dimensional (3D) images and analyze the bone volume/tissue volume (BV/TV).

2.10. Calvaria bone histological analysis and immunofluorescence staining

After micro-CT scanning, the calvarial bones were decalcified in 10% EDTA (pH = 7.4) for 2 weeks, dehydrated, embedded in paraffin, and sectioned at a thickness of 5 μm for hematoxylin and eosin (H&E) staining and TRAP staining (Servicebio, Wuhan, China). The percentage of the bone erosion area and the number of TRAP-positive osteoclasts were quantified. For immunofluorescence staining, the collected calvaria bones were embedded in optimal cutting temperature (OCT) compound (Sakura Finetek, CA, USA). Serial 5 μm thick sections were cut and permeabilized with 0.1% Triton X-100. After being blocked with serum-based blocking buffer for 60 min, the slides were incubated with primary antibodies against CD86 (Novus Biologicals, CO, USA), iNOS (Abcam, Cambridge, UK) or Arg1 (Cell Signaling Technology, MA, USA) overnight at 4 °C. After the slides were incubated with secondary antibodies for 60 min at room temperature, the slides were mounted with FluoroShield mounting medium containing DAPI (Abcam, Cambridge, UK). $CD68^+iNOS^+$ and $CD68^+Arg1^+$ macrophages were observed using a laser-scanning confocal microscope (Zeiss LSM 900, Zeiss, Germany).

2.11. Real-time polymerase chain reaction (RT–PCR)

Total RNA was isolated from LPS- or RANKL-treated RAW264.7 cells using an RNA-Quick Purification Kit (ESscience, Beijing, China) according to the manufacturer's instructions. Small RNA was isolated from Nor-sEV and Hypo-sEV using the Exosome RNA Purification Kit (ESscience, Beijing, China) according to the manufacturer's instructions. For real-time PCR analysis of mRNA, complementary DNA (cDNA) was synthesized using the PrimeScript™ RT Reagent Kit (TaKaRa Co., Kyoto, Japan). Real-time PCR was performed using Fast SYBR Green Master Mix (Thermo Fisher, Waltham, MA, USA) and gene-specific primers. The primers used are listed in Supplementary Table S1. The relative mRNA expression levels were normalized to that of *β-actin* following the $2^{-\Delta\Delta}$CT comparative method. For real-time PCR analysis of mature miRNAs, cDNA synthesis of miRNA and subsequent real-time PCR were performed using the All-in-One™ miRNA qRT–PCR Detection Kit (Genecopoeia, Guangzhou, China). Rnu6 small nuclear RNA (snRNA) was used as an endogenous control. The relative expression levels of miRNAs were normalized to Rnu6 following the $2^{-\Delta\Delta CT}$ comparative method. The primers for miRNA analysis were purchased from GeneCopoeia (Guangzhou, China).

2.12. Flow cytometric analysis of macrophage surface markers

RAW264.7 macrophages were stimulated with 500 ng/mL LPS (Sigma–Aldrich, MO, USA) in the presence and absence of 30 μg/mL Nor-sEV and Hypo-sEV for 12 h. Then, RAW264.7 cells were washed with PBS, treated with TrypLE (Gibco, USA) and resuspended in 0.5 mL of PBS supplemented with 5% FBS. Macrophage surface marker expression was analyzed by flow cytometry (BD Bioscience, San Jose,

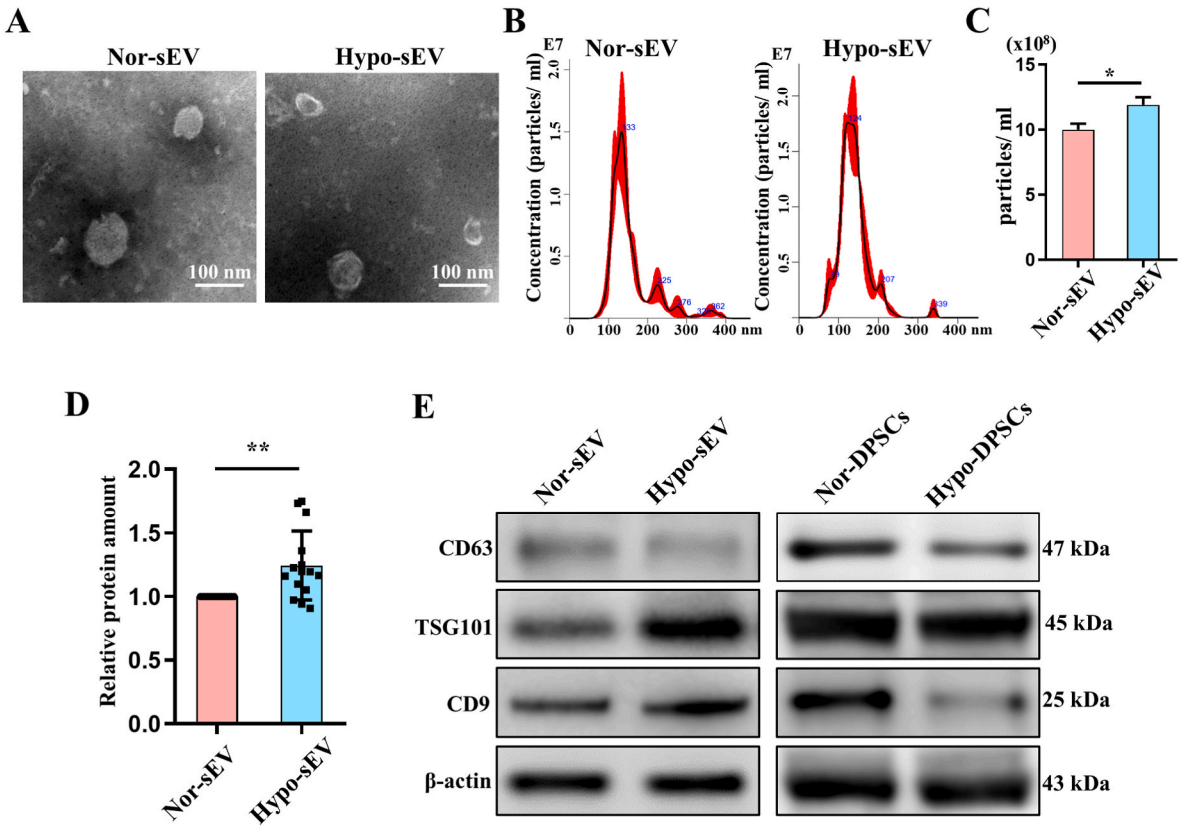

Fig. 1. Characterization of DPSCs-sEV under normoxic (Nor-sEV) or hypoxic (Hypo-sEV) conditions. (A) The ultrastructures of Nor-sEV and Hypo-sEV were observed using transmission electron microscopy (TEM). **(B)** The size distribution of purified Nor-sEV and Hypo-sEV was assessed using nanoparticle tracking analysis (NTA). **(C)** NTA showing the concentrations of Nor-sEV and Hypo-sEV (n = 3). **(D)** The protein concentrations of Nor-sEV and Hypo-sEV were determined using a BCA assay. **(E)** The expression of the sEV-associated protein markers CD63, TSG101 and CD9 in purified Nor-sEV and Hypo-sEV, and DPSCs cultured under normoxic or hypoxic conditions were determined by western blotting. Error bars represent the mean ± s.d. $^{**}P < 0.01$; $^{*}P < 0.05$.

CA, USA) after the samples were stained with CD86-PerCP, CD163-APC and CD206-FITC monoclonal antibodies (eBioscience, San Diego, CA, USA) for 30 min in the dark at 4 °C.

2.13. Osteoclast differentiation in vitro

To investigate the effects of Nor-sEV or Hypo-sEV on osteoclast differentiation, RAW264.7 cells (passages 5–15; ATCC, Manassas, VA) were stimulated with 50 ng/mL soluble recombinant RANKL (R&D Systems, Minneapolis, MN, USA) for 4 days in the presence or absence of 30 μg/mL Nor-sEV or Hypo-sEV. Then, the cells were subjected to TRAP staining (Servicebio, China) according to the manufacturer's protocol. In brief, the cells were fixed with 4% paraformaldehyde for 15 min, permeabilized with 0.1% Triton X-100 for 20 min, incubated with TRAP staining solution in the dark at 37 °C for 1 h, and then stained with DAPI solution (KeyGen Biotech, Nanjing, China) in the dark at 37 °C for 15 min. TRAP-positive multinucleated cells with more than three nuclei were considered as osteoclasts, which were imaged by an optical fluorescence microscope (Olympus, Japan).

2.14. sEV uptake by RAW264.7 cells

PKH67 (Sigma, USA) was used to label Nor-sEV and Hypo-sEV with green fluorescence according to the manufacturer's instructions. For investigation of whether RAW264.7 cells could uptake the two types of sEV, PKH67-labeled Nor-sEV and Hypo-sEV were incubated with RAW264.7 cells. After 24 h of coculture, RAW264.7 cells were fixed with 4% paraformaldehyde for 20 min, permeabilized with 0.1% Triton X-100 in PBS for 10 min, and incubated with ActinRed™ 555 ReadyProbes™ (Invitrogen, USA) for 30 min and DAPI for 5 min. The cellular uptake of sEV was observed with a fluorescence microscope (Zeiss, Germany).

2.15. MicroRNA sequencing

Small RNAs were extracted from Nor-sEV and Hypo-sEV and used for miRNA sequencing. Three biological replicates derived from three independent rats for each sEV were used. MiRNA libraries were constructed and then subjected to deep sequencing via an Illumina Hi-Seq 2500 platform at RiboBio Co. Ltd. (Guangzhou, China). Differentially expressed miRNAs with a 1.5-fold change in expression ($p < 0.05$) were analyzed. Then, Kyoto Encyclopedia of Genes (KEGG) pathway analysis and Gene Ontology (GO) analysis of the target mRNA genes of the differentially expressed miRNAs were performed.

2.16. Small-interfering RNA (siRNA)-mediated knockdown and microRNA mimic and inhibitor transfection

RAW264.7 cells (3×10^5) were seeded on a 6-well culture plate and transfected with miR-210-3p mimics (50 μM; RiboBio, China), inhibitors (100 μM; RiboBio, China) or NF-κB1 siRNA (20 μM; RiboBio, China) using Lipofectamine RNAiMAX transfection reagent (Life Technologies, CA, USA) in Opti-MEM (Life Technologies) according to the manufacturer's instructions. Nontargeting control siRNAs (RiboBio, China) were used as negative controls. After 48 h of transfection, the level of miR-210-3p was determined by RT–PCR, and NF-κB1 knockdown was confirmed by western blotting and RT–PCR.

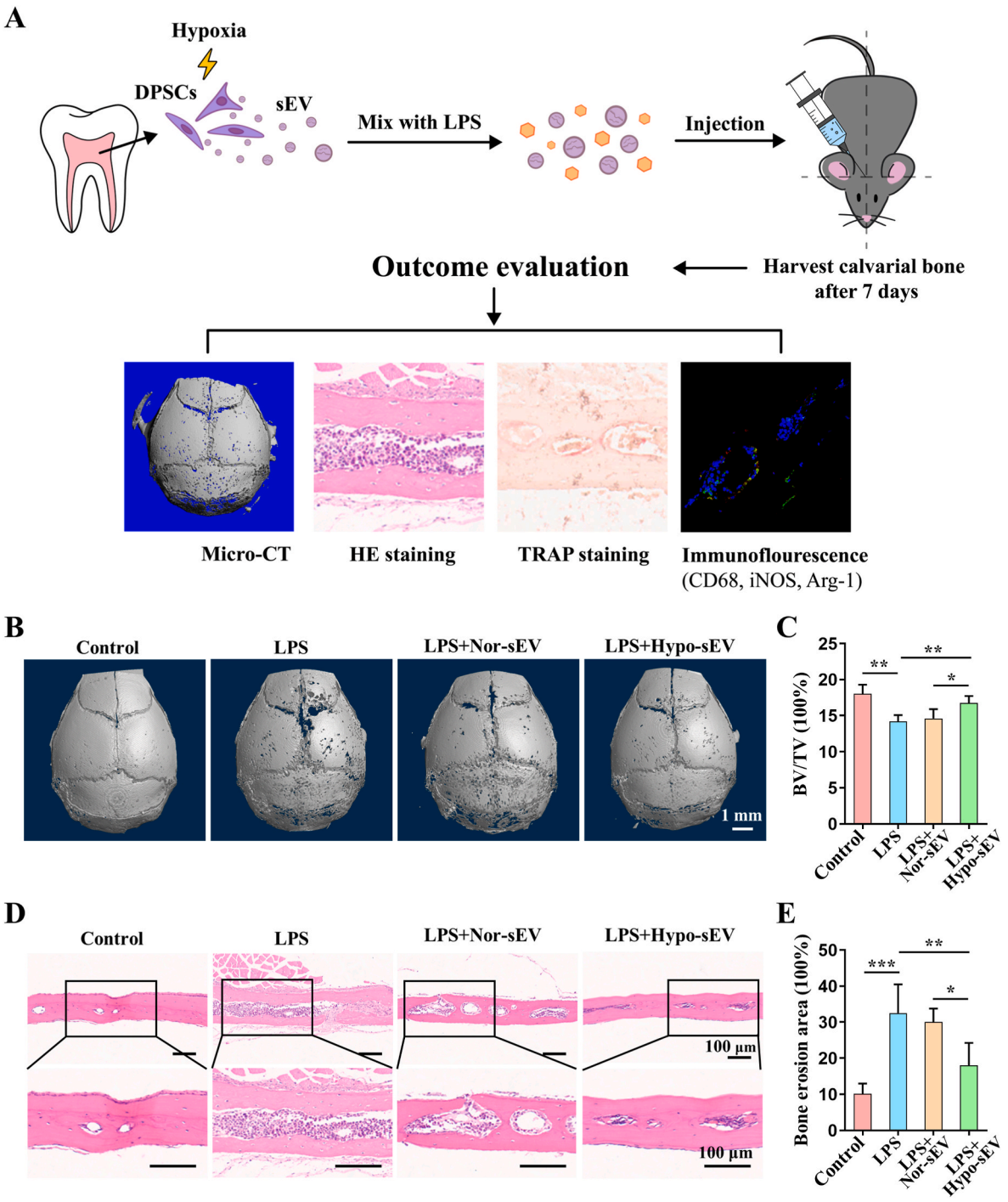

Fig. 2. Hypo-sEV inhibit LPS-induced inflammatory calvarial bone loss *in vivo*. (A) Schematic representations showing Nor-sEV and Hypo-sEV injection in mice with LPS-induced calvarial bone loss. **(B)** Micro-CT scanning and subsequent 3D reconstruction of the calvarial bone after treatment with LPS and Nor-sEV or Hypo-sEV (n = 5). **(C)** BV/TV (bone volume/total volume) was recorded. **(D)** H&E staining showing calvarial destruction and inflammatory cell infiltration. **(E)** The percentage of the bone erosion area in the calvarial bone matrix was determined. Error bars represent the mean ± s.d. $^{***}P < 0.005$; $^{**}P < 0.01$; $^{*}P < 0.05$.

2.17. Dual-luciferase reporter assay

Luciferase reporter constructs encoding the wild-type 3′UTR of NF-κB1 (NF-κB1-WT) or mutant 3′UTR of NF-κB1 (NF-κB1-MUT) were synthesized. Then, 293T cells were transfected with the 3′UTR luciferase vector and miR-210-3p mimics using Lipo 6000 (Beyotime Biotechnology, Shanghai, China) for 24 h. Luciferase activities were analyzed with a Dual-Glo® Luciferase Assay System (Promega, WI, USA) according to the manufacturer's protocol.

2.18. Statistical analysis

All results are expressed as the mean ± standard deviation (SD). Statistical analysis was performed using Student's *t*-test or one-way analysis of variance (ANOVA). *P* values less than 0.05 were considered statistically significant.

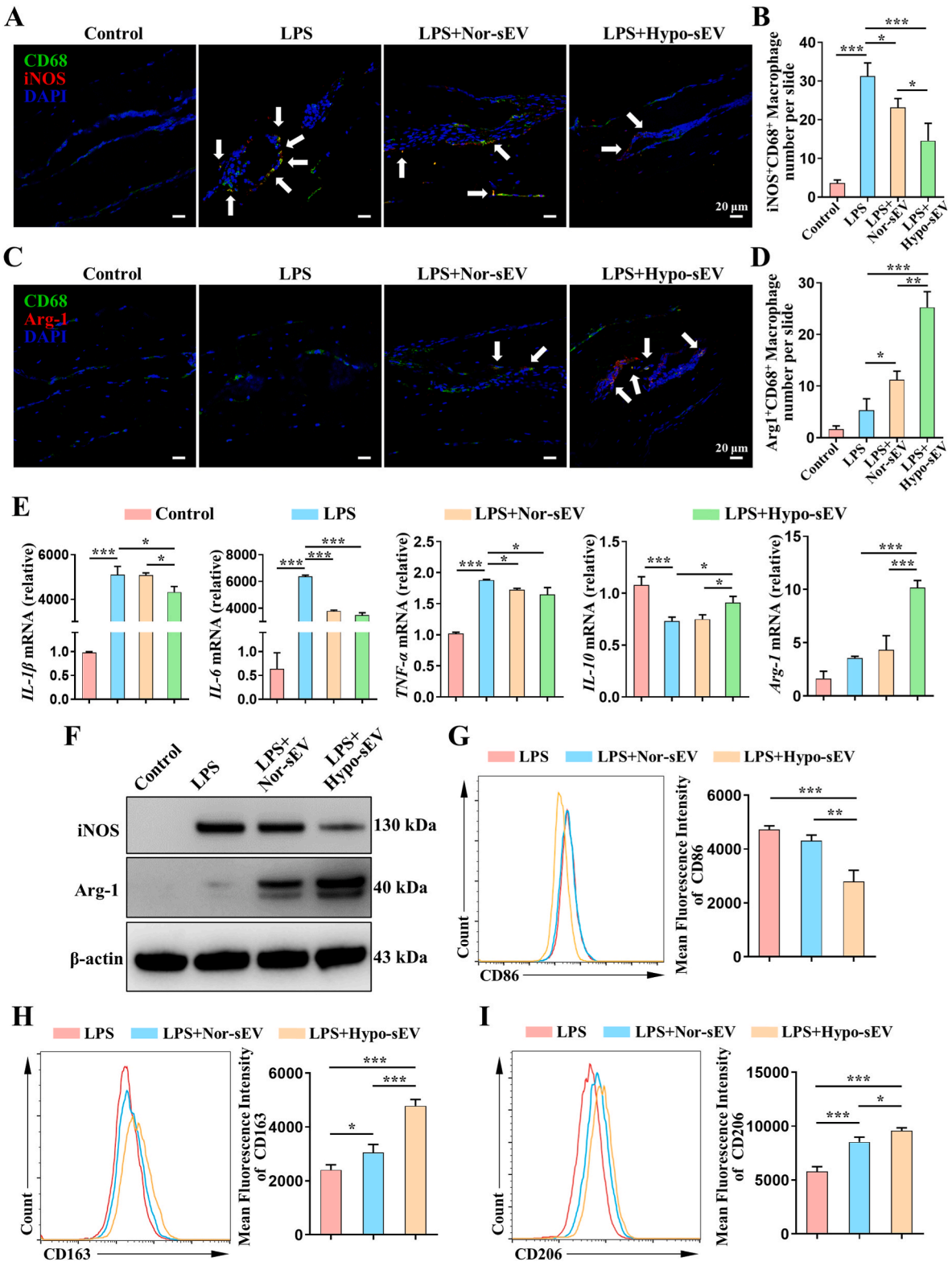

Fig. 3. Hypo-sEV show increased potential to induce M2 macrophage generation compared with Nor-sEV *in vivo* and *in vitro*. (A) $CD68^{+}iNOS^{+}$ macrophages in calvarial bone matrix after treatment with LPS with Nor-sEV or Hypo-sEV were observed using laser-scanning confocal microscope (white arrow) (n = 5). **(B)** Statistical analysis of the number of $CD68^{+}iNOS^{+}$ macrophages. **(C)** $CD68^{+}Arg1^{+}$ macrophages in the calvarial bone matrix were observed using a laser-scanning confocal microscope (white arrow). **(D)** Statistical analysis of the number of $CD68^{+}Arg1^{+}$ macrophages. **(E)** qPCR analysis of the relative mRNA levels of the macrophage polarization-related factors *IL-1β*, *IL-6*, *TNF-α*, *IL-10* and *Arg1* in Nor-sEV- or Hypo-sEV-treated RAW264.7 cells in the presence of LPS. **(F)** LPS-treated RAW264.7 cells were stimulated with Nor-sEV or Hypo-sEV for 24 h. The expression of iNOS and Arg1 was determined by western blotting. **(G-I)** The expression or fluorescence intensity of the macrophage polarization markers CD86, CD163 and CD206 on the surface of LPS-treated RAW264.7 cells was assessed using flow cytometry. Error bars represent the mean ± s.d. $^{***}P < 0.005$; $^{**}P < 0.01$; $^{*}P < 0.05$.

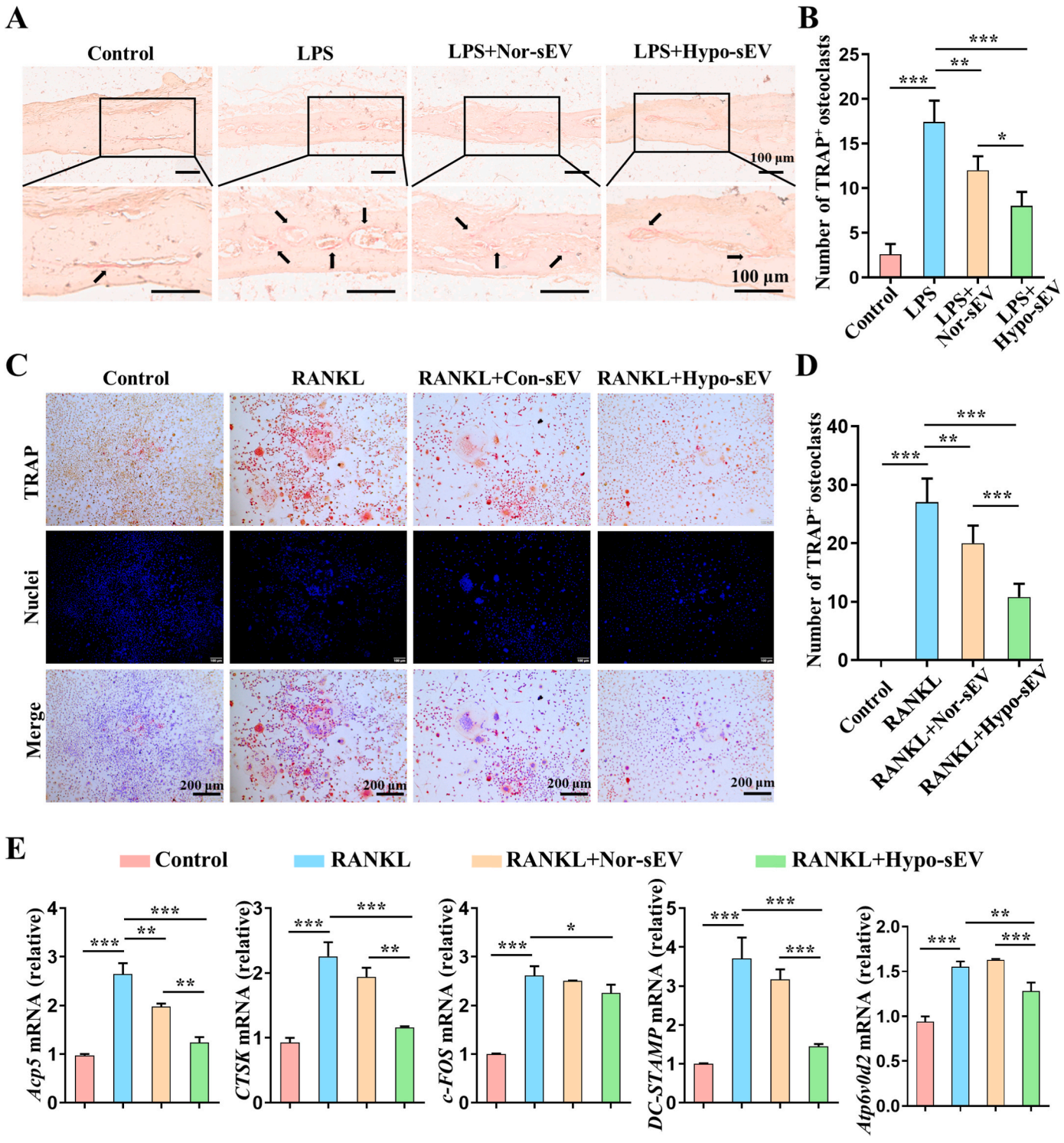

Fig. 4. Hypo-sEV exhibited better efficacy in inhibiting osteoclast formation than Nor-sEV *in vivo* and *in vitro*. (A) Osteoclasts in the calvarial bone matrix after treatment with LPS with Nor-sEV or Hypo-sEV were visualized using TRAP staining (dark arrow) (n = 5). **(B)** The histogram shows the number of $TRAP^+$ osteoclasts in the calvarial bone matrix. **(C)** RAW264.7 cells were stimulated for 4 days with 50 ng/mL RANKL to induce osteoclast formation in the presence of Nor-sEV or Hypo-sEV, and then subjected to TRAP staining. **(D)** $TRAP^+$ multinucleated cells containing 3 or more nuclei were counted as osteoclasts. **(E)** qPCR analysis showed the relative mRNA levels of the osteoclastogenesis-associated genes *Acp5*, *CTSK*, *c-FOS*, *DC-STAMP* and *Atp6v0d2* in RANKL-treated RAW264.7 cells in the presence of Nor-sEV or Hypo-sEV. Error bars represent the mean ± s.d. $^{***}P < 0.005$; $^{**}P < 0.01$; $^{*}P < 0.05$.

3. Results

3.1. Characterization of DPSCs, Nor-sEV and Hypo-sEV

As shown in Fig. S1A, flow cytometry demonstrated that the isolated DPSCs were positive for the expression of MSC surface markers, including CD29, CD44 and CD90, with frequencies up to 96.9%, but were negative for the expression of the hematopoietic markers CD34 and CD45, with a frequency less than 3.2%. Immunofluorescence analysis showed that DPSCs were positive for the MSC marker vimentin but

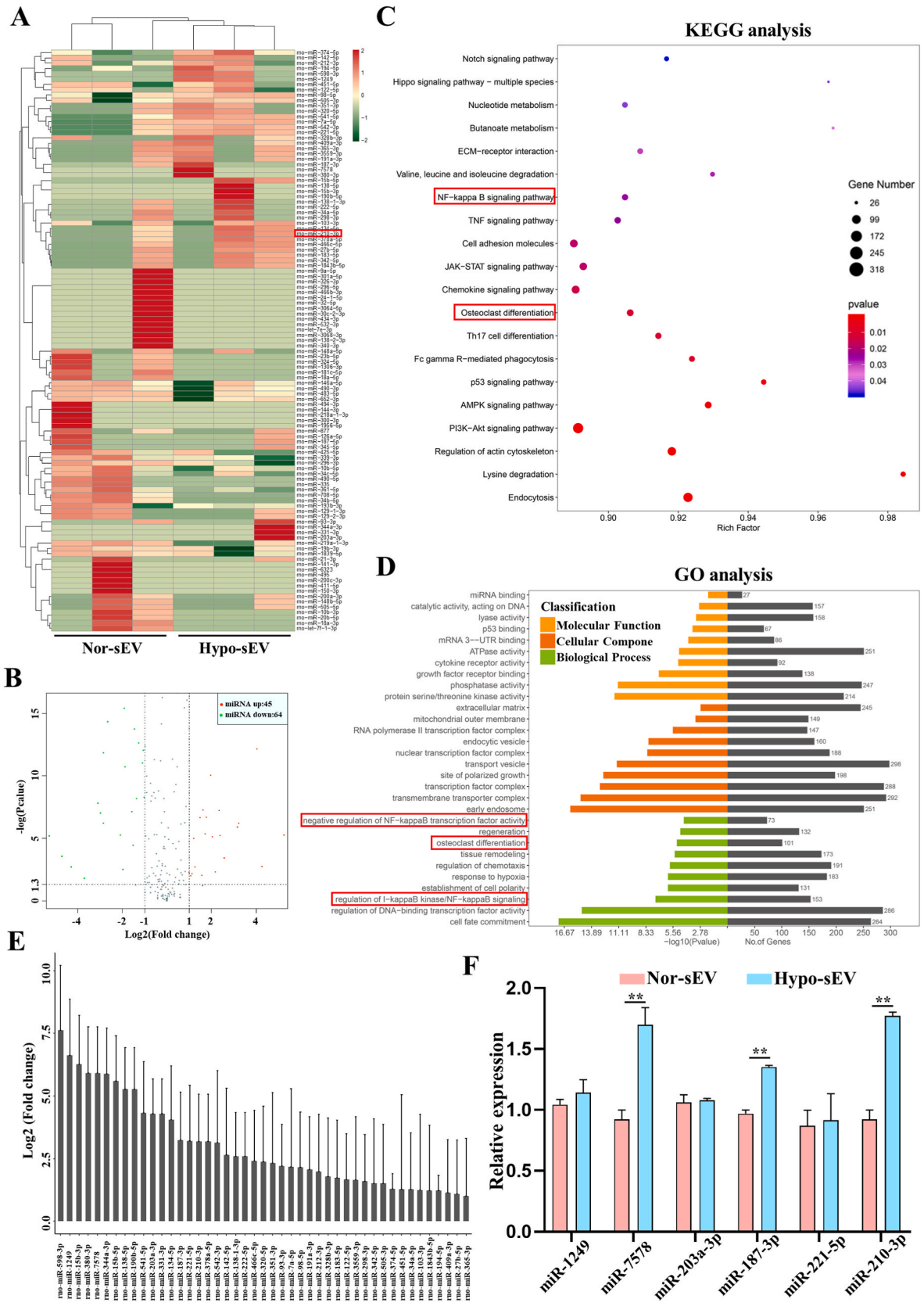

Fig. 5. Hypoxia significantly changes the miRNA profiles of DPSC-sEV. (A) Heatmap showing the 45 upregulated and 64 downregulated miRNAs with a ≥1.5-fold difference between Nor-sEV and Hypo-sEV (n = 3). **(B)** Volcano plot showing significantly upregulated (red dots) and downregulated (green dots) miRNAs in Hypo-sEV, compared with Nor-sEV. **(C)** Kyoto Encyclopedia of Genes and Genomes (KEGG) pathway enrichment analysis and **(D)** Gene Ontology (GO) analysis of the target mRNAs of the differentially expressed miRNAs. **(E)** The histogram shows the upregulated miRNAs in Hypo-sEV. **(F)** qPCR analysis showed the levels of miR-1249, miR-7578, miR-203a-3p, miR-187-3p, miR-221-5p and miR-210-3p in Nor-sEV and Hypo-sEV. Error bars represent the mean ± s.d. $^{**}P < 0.01$.

negative for the epithelial marker cytokeratin (Fig. S1B). Furthermore, DPSCs formed mineralized matrix that were visualized by alizarin red staining after osteogenic induction for 14 days. Lipid droplet formation, as visualized by Oil Red O staining, was also observed in DPSCs after adipogenic induction for 14 days (Figs. S1C and D). These results indicated that cultured DPSCs possessed the mesenchymal phenotype of MSCs with multipotent differentiation capacity.

Nor-sEV and Hypo-sEV were isolated from the supernatant of DPSCs and hypoxia-preconditioned DPSCs, respectively, using ultracentrifugation. Using TEM, we observed that both sEV exhibited classic cup-shaped morphology (Fig. 1A). NTA showed that the peak diameters of Nor-sEV and Hypo-sEV were 133 nm and 124 nm, respectively (Fig. 1B). Moreover, we found that Hypo-sEV exhibited increased concentrations or particles compared with that of Nor-sEV (Fig. 1C). The protein concentration of Hypo-sEV was also significantly higher than that of Nor-sEV (Fig. 1D). We used Western blot analysis to confirm that the two types of purified sEV expressed the sEV-associated protein markers CD63, TSG101 and CD9. Furthermore, the expression levels of TSG101 and CD9 in Hypo-sEV were higher than those in Nor-sEV (Fig. 1E). Interestingly, hypoxia significantly decreased the expression of CD63 and CD9 in DPSCs (Fig. 1E), indicating that hypoxia induced the release of sEV from DPSCs rather than affecting sEV generation in DPSCs.

3.2. Hypo-sEV ameliorate LPS-induced inflammatory bone loss in vivo

To investigate the therapeutic effect of Nor-sEV and Hypo-sEV on inflammatory osteolysis *in vivo*, we used an LPS-induced inflammatory bone loss model (Fig. 2A). Micro-CT scanning and 3D reconstruction of calvarial bones showed that mice in the LPS group exhibited excessive bone loss with a significant decrease in the BV/TV compared with those in the control group (Fig. 2B and C). Histological analysis also indicated increased bone erosion areas with rampant inflammatory cell infiltration after LPS injection (Fig. 2D and E). Nor-sEV failed to show significant therapeutic effects on LPS-induced osteolysis, as assessed by micro-CT scanning and histological examination, although a slight increase in the BV/TV and decreased bone erosion areas were observed in the Nor-sEV group (Fig. 2B–E). In contrast, Hypo-sEV rescued LPS-induced inflammatory osteolysis in the calvarial bone matrix in terms of increasing the BV/TV and decreasing bone erosion areas, as demonstrated by micro-CT scanning and H&E staining analysis (Fig. 2B–E). These results indicate that Hypo-sEV significantly ameliorated LPS-induced inflammatory bone loss *in vivo*.

3.3. Hypo-sEV induce macrophage M2 polarization in vivo and in vitro

M2 macrophages play an essential role in tissue inflammation resolution and facilitate osteogenesis, angiogenesis and bone repair through the release of anti-inflammatory cytokines and growth factors [28–30]. Since the shift of proinflammatory macrophages toward an anti--inflammatory M2 phenotype promotes bone repair, we next examined whether Hypo-sEV could induce macrophage M2 polarization *in vivo*. Immunofluorescence analysis indicated that LPS significantly increased the number of $CD68^+iNOS^+$ macrophages (M1 macrophages), which was suppressed by Nor- and Hypo-sEV. (Fig. 3A and B, Fig. S2A). The LPS + Hypo-sEV group and LPS + Nor-sEV group showed more $CD68^+Arg1^+$ macrophages (M2 macrophages) in the calvarial bone matrix than the LPS group (Fig. 3C, D, Fig. S2B). In addition, fewer $CD68^+iNOS^+$ macrophages and more $CD68^+Arg1^+$ macrophages were present in the LPS+Hypo-sEV group than in the LPS + Nor-sEV group (Fig. 3A–D). To further determine the effects of the two types of sEV on macrophage inflammatory responses and phenotypic conversion *in vitro*, we incubated LPS-treated RAW264.7 cells with Nor-sEV or Hypo-sEV. LPS treatment resulted in a striking increase in the mRNA expression of the proinflammatory cytokines *IL-1β*, *IL-6* and *TNF-α* and a decrease in the mRNA expression of the anti-inflammatory cytokine *IL-10*. Nor-sEV inhibited the expression of *IL-6* and *TNF-α* without an obvious effect on *IL-1β* or *IL-10* expression. Hypo-sEV treatment not only inhibited the expression of *IL-1β*, *IL-6* and *TNF-α*, but also upregulated the expression of *IL-10*, as well as *Arg*1, which is a key effector and marker of M2 macrophages. Moreover, compared with Nor-sEV, Hypo-sEV significantly suppressed the expression of *IL-1β* and promoted the expression of *IL-10* and *Arg1* (Fig. 3E). Using western blotting and flow cytometry, we found that Nor-sEV upregulated the expression of the M2 macrophage markers Arg1, CD163 and CD206 in LPS-stimulated RAW264.7 cells (Fig. 3F, H, I). However, no obvious change in the expression of the M1 macrophage markers iNOS and CD86 was observed (Fig. 3F and G). In contrast, Hypo-sEV showed superior efficacy in inducing the expression of Arg1, CD163 and CD206 relative to Nor-sEV (Fig. 3F, H, I). Furthermore, Hypo-sEV evidently inhibited the expression of iNOS and CD86 (Fig. 3F and G). These results indicate that Hypo-sEV can inhibit the LPS-induced macrophage inflammatory response and induce M2 macrophage polarization.

3.4. Hypo-sEV inhibit osteoclastogenesis in vivo and in vitro

Inflammatory bone resorption was caused by excessive osteoclast formation [31,32]. Therefore, we next examined whether Hypo-sEV inhibited osteoclastogenesis *in vivo*. TRAP staining analysis demonstrated that LPS treatment resulted in a marked increase in the number of $TRAP^+$ osteoclasts in calvarial bones, which was consistent with enhanced osteolysis. Both Nor-sEV and Hypo-sEV decreased the number of TRAP-positive osteoclasts induced by LPS (Fig. 4A and B). Furthermore, the number of TRAP-positive osteoclasts in the Hypo-sEV group was lower than that in the Nor-sEV group (Fig. 4B). To further investigate whether the two types of sEV could directly inhibit osteoclast differentiation, we incubated RANKL-treated RAW264.7 cells with Nor-sEV or Hypo-sEV *in vitro*. RAW264.7 cells cultured in the presence of RANKL matured into numerous, $TRAP^+$ multinucleated osteoclasts (Fig. 4C). In contrast, Nor-sEV and Hypo-sEV suppressed osteoclast differentiation induced by RANKL, as shown by the decreased number of osteoclasts. Moreover, the inhibitory effect on osteoclastogenesis in the Hypo-sEV treatment group was superior to that in the Nor-sEV treatment group (Fig. 4C and D). The effects of the two types of sEV on the levels of specific osteoclastogenesis-related genes were also determined in RAW264.7 cells stimulated with RANKL. We found that under RANKL stimulation, there was an appreciable increase in the mRNA expression of tartrate-resistant acid phosphatase 5 (Acp5), cathepsin K (CTSK), c-FOS, dendritic cell-specific transmembrane protein (DC-STAMP) and ATPase H^+ Transporting V0 Subunit D2 (Atp6v0d2). Nor-sEV only significantly inhibited the expression of *Acp5*, although the expression of *CTSK*, *c-FOS* and *DC-STAMP* showed a tendency toward declines after Nor-sEV treatment. Notably, Hypo-sEV significantly inhibited the expression levels of *Acp5*, *CTSK*, *c-FOS*, *DC-STAMP* and *Atp6v0d2* induced by RANKL. RANKL-treated RAW264.7 cells exposed to Hypo-sEV also exhibited lower expression levels of *Acp5*, *CTSK*, *DC-STAMP* and *Atp6v0d2* than those exposed to Nor-sEV (Fig. 4E). These data indicate that Hypo-sEV directly inhibit osteoclastogenesis *in vivo* and *in vitro*.

3.5. Hypoxia significantly alters the miRNA profiles of DPSC-sEV

Our above findings prompted us to further identify the components within Hypo-sEV that exert regulatory effects on the macrophage inflammatory response and osteoclastogenesis. As an important component of sEV, miRNAs have been demonstrated to play critical roles in sEV-mediated biological functions [10]. Therefore, we analyzed the miRNA profiles of Nor-sEV and Hypo-sEV using next-generation sequencing. Compared with those in Nor-sEV, 45 miRNAs were upregulated and 64 miRNAs were downregulated in Hypo-sEV (Fig. 5A and B). Kyoto Encyclopedia of Genes and Genomes (KEGG) signaling pathway enrichment analysis showed that the target mRNAs of the differentially expressed miRNAs were enriched in the NF-κB signaling

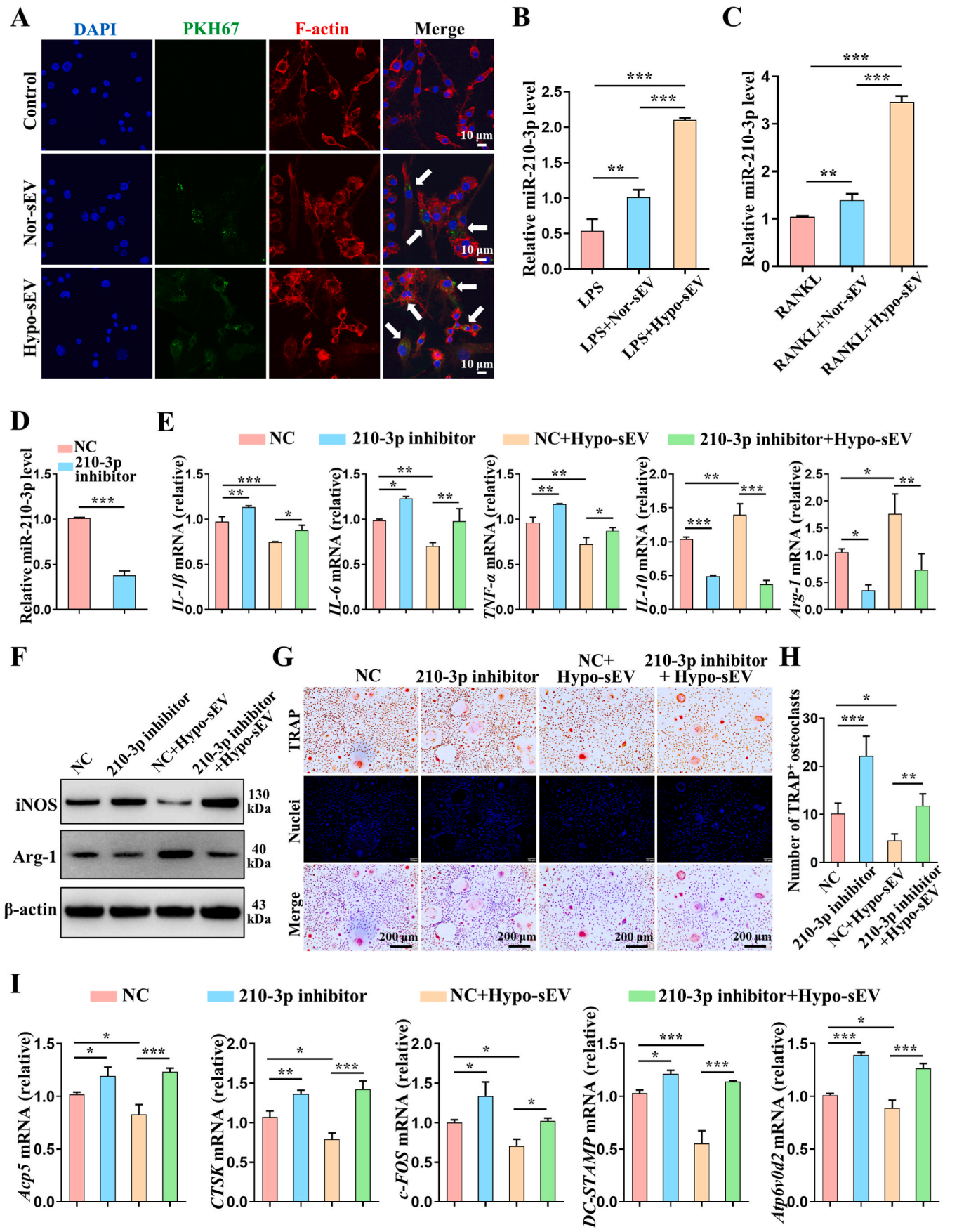

(caption on next page)

Fig. 6. Hypo-sEV induce M2 macrophage polarization and inhibit osteoclastogenesis by delivering miR-210-3p *in vitro*. (A) RAW264.7 cells were treated with PKH67-labeled Nor-sEV or Hypo-sEV for 24 h *in vitro*. The uptake of Nor-sEV or Hypo-sEV was observed by ActinGreen™ 555 ReadyProbes™ Reagent staining of F-actin in the cytoplasm of RAW264.7 cells (white arrow). **(B, C)** qPCR analysis showing the levels of miR-210-3p in LPS- or RANKL-treated RAW264.7 cells exposed to Nor-sEV or Hypo-sEV. **(D)** qPCR analysis showing the expression level of miR-210-3p in RAW264.7 cells treated with the miR-210-3p inhibitor. **(E)** qPCR analysis showing the relative mRNA levels of the macrophage polarization-related factors *IL-1β*, *IL-6*, *TNF-α*, *IL-10* and *Arg1* in LPS-treated RAW264.7 cells that were cultured with Hypo-sEV and the miR-210-3p inhibitor. **(F)** The expression of iNOS and Arg1 in LPS-treated RAW264.7 cells that were cultured with Hypo-sEV and the miR-210-3p inhibitor was determined using western blotting. **(G)** TRAP staining in RANKL-treated RAW264.7 cells in the presence of Hypo-sEV and the miR-210-3p inhibitor. **(H)** The histogram shows the number of $TRAP^+$ osteoclasts. **(I)** qPCR analysis showing the relative mRNA levels of the osteoclastogenesis-associated genes *Acp5*, *CTSK*, *c-FOS*, *DC-STAMP* and *Atp6v0d2* in RANKL-treated RAW264.7 cells exposed to Hypo-sEV and the miR-210-3p inhibitor. Error bars represent the mean ± s.d. $^{***}P < 0.005$; $^{**}P < 0.01$; $^{*}P < 0.05$.

pathway, cell adhesion molecules, chemokine signaling pathway, osteoclast differentiation, regulation of actin cytoskeleton and endocytosis pathways that could regulate inflammatory response and osteoclast formation (Fig. 5C). Furthermore, Gene Ontology (GO) analysis revealed that the analyzed target mRNAs could well modulate cell behaviors by affecting biological processes (including negative regulation of NF-κB transcription factor activity, regulation of NF-κB signaling, regeneration, osteoclast differentiation, tissue remodeling, response to hypoxia, establishment of cell polarity as well as regulation of DNA-binding transcription factor activity), regulating cellular component in RNA polymerase II transcription factor complex, site of polarized growth and transcription factor complex, and adjusting molecular function in miRNA binding, acting on DNA, mRNA 3′UTR binding, cytokine receptor activity, ATPase activity, and phosphatase activity (Fig. 5D). Next, we validated the expression of miRNAs that have been shown to be associated with the macrophage inflammatory response or osteoclast differentiation among the top 20 significantly upregulated miRNAs in Hypo-sEV, including miR-1249 [33], miR-7578 [34], miR-203a-3p [35], miR-187-3p [36], miR-221-5p [37] and miR-210-3p [38] (Fig. 5E). The PCR results indicated that Hypo-sEV showed increased levels of miR-7578, miR-187-3p and miR-210-3p compared with Nor-sEV (Fig. 5F).

3.6. Hypo-sEV induce M2 macrophage polarization and inhibit osteoclastogenesis by upregulating miR-210-3p expression in vitro

We then examined the potential of miR-7578, miR-187-3p and miR-210-3p to inhibit the macrophage inflammatory response using corresponding miRNA mimics. We found that miR-7578 mimic treatment induced the expression of IL-1β, IL-6 and TNFα (Figs. S3A and B). MiR-187-3p mimic treatment significantly inhibited IL-6 and TNF-α expression but increased IL-1β expression (Figs. S3C and D). Interestingly, the miR-210-3p mimic inhibited the expression of IL-1β and IL-6 while inducing the expression of IL-10 in RAW264.7 cells regardless of the presence or absence of LPS (Figs. S4A and B). The miR-210-3p mimic also downregulated TNF-α and iNOS expression but upregulated Arg-1 expression in LPS-treated RAW264.7 cells (Figs. S4B and C). These data suggest the key role of miR-210-3p in mediating the therapeutic effects of Hypo-sEV.

To further confirm whether enriched miR-210-3p within Nor-sEV or Hypo-sEV could be delivered to macrophages and osteoclasts and contribute to the suppressive effects of Nor-sEV and Hypo-sEV on the macrophage inflammatory response and osteoclastogenesis, we next cocultured RAW264.7 cells with PHK-67-labeled Nor-sEV or Hypo-sEV. Immunofluorescence analysis confirmed that Nor-sEV and Hypo-sEV were endocytosed by RAW264.7 cells (Fig. 6A). In addition, after treatment with Nor-sEV or Hypo-sEV, miR-210-3p levels significantly increased in the LPS- or RANKL-treated RAW264.7 cells. Notably, compared with the LPS- or RANKL-treated RAW264.7 cells cocultured with Nor-sEV, the cells cocultured with Hypo-sEV showed upregulated miR-210-3p expression (Fig. 6B and C). These data suggest that Hypo-sEV can deliver miR-210-3p into macrophages and osteoclasts. To confirm the functional role of miR-210-3p, we reduced miR-210-3p levels with a miR-210-3p inhibitor (Fig. 6D), which significantly promoted the expression of IL-1β, IL-6, TNF-α and iNOS while decreasing the expression of IL-10 and Arg1 in LPS-treated RAW264.7 cells (Fig. 6E and F). More importantly, the miR-210-3p inhibitor attenuated the capacities of Hypo-sEV to induce M2 macrophage polarization in terms of decreasing IL-1β, IL-6, TNF-α and iNOS expression, as well as upregulating IL-10 and Arg1 expression (Fig. 6E and F).

Furthermore, RANKL-treated RAW264.7 cells incubated with the miR-210-3p inhibitor resulted in an increased number of $TRAP^+$ multinucleated osteoclasts, as well as increased expression of Acp5, CTSK, c-FOS, DC-STAMP and Atp6v0d2 (Fig. 6G–I). The miR-210-3p inhibitor also partially decreased the ability of Hypo-sEV to inhibit the formation of $TRAP^+$ osteoclasts and the expression of the osteoclastogenesis-related genes Acp5, CTSK, c-FOS, DC-STAMP and Atp6v0d2 (Fig. 6G–I). Conversely, the miR-210-3p mimic inhibited the formation of $TRAP^+$ multinucleated osteoclasts, as well as the expression of Acp5, CTSK, c-FOS, and DC-STAMP, in RANKL-treated RAW264.7 cells (Figs. S4D–F). Collectively, these results suggest that Hypo-sEV induce M2 macrophage polarization and inhibit osteoclastogenesis by upregulating miR-210-3p expression.

3.7. MiR-210-3p within Hypo-sEV ameliorates LPS-induced inflammatory bone loss in vivo

To further confirm whether miR-210-3p mediates the observed therapeutic effects of Hypo-sEV *in vivo*, we used antagomir-210-3p in an LPS-induced inflammatory bone loss model. Micro-CT scanning and histological analysis revealed that antagomir-210-3p markedly abrogated the therapeutic effects of Hypo-sEV on LPS-induced inflammatory bone loss, as indicated by the decreased BV/TV and enhanced inflammatory cell infiltration and bone erosion areas (Fig. 7A–D). Furthermore, immunofluorescence analysis indicated that compared with those in the LPS + Antagomir-NC + Hypo-sEV group, more $CD68^+iNOS^+$ macrophages and fewer $CD68^+Arg^+$ macrophages were present in the calvarial bone matrix in the LPS + Antagomir-210-3p + Hypo-sEV group (Fig. 7E–H, Figs. S5A and B). Likewise, TRAP staining showed that the number of $TRAP^+$ osteoclasts in calvarial bones in the LPS+Antagomir-210-3p + Hypo-sEV group was higher than that in the LPS + Antagomir-NC + Hypo-sEV group (Fig. 7I and J). These results indicate that miR-210-3p within Hypo-sEV significantly ameliorated LPS-induced inflammatory osteolysis *in vivo* by inducing M2 macrophage polarization and inhibiting osteoclast formation.

3.8. MiR-210-3p within Hypo-sEV targets NF-κB1

Since activation of the NF-κB pathway is critical for M1 macrophage polarization and osteoclastogenesis [39,40], we investigated the effects of Hypo-sEV on the NF-κB pathway in LPS- or RANKL-treated RAW264.7 cells. Treatment with LPS or RANKL increased the expression of NF-κB1 (also known as p105, the precursor of p50) and p50 at the protein and mRNA levels in RAW264.7 cells, and this effect was downregulated by Hypo-sEV (Fig. 8A and B). With regard to the key role of miR-210-3p in Hypo-sEV-mediated therapeutic effects, we next asked whether miR-210-3p modulated the macrophage inflammatory response and osteoclast formation by inhibiting NF-κB1. The Western blot and PCR results showed that miR-210-3p inhibitor treatment significantly upregulated the expression of p105 and p50 in LPS- or RANKL-treated

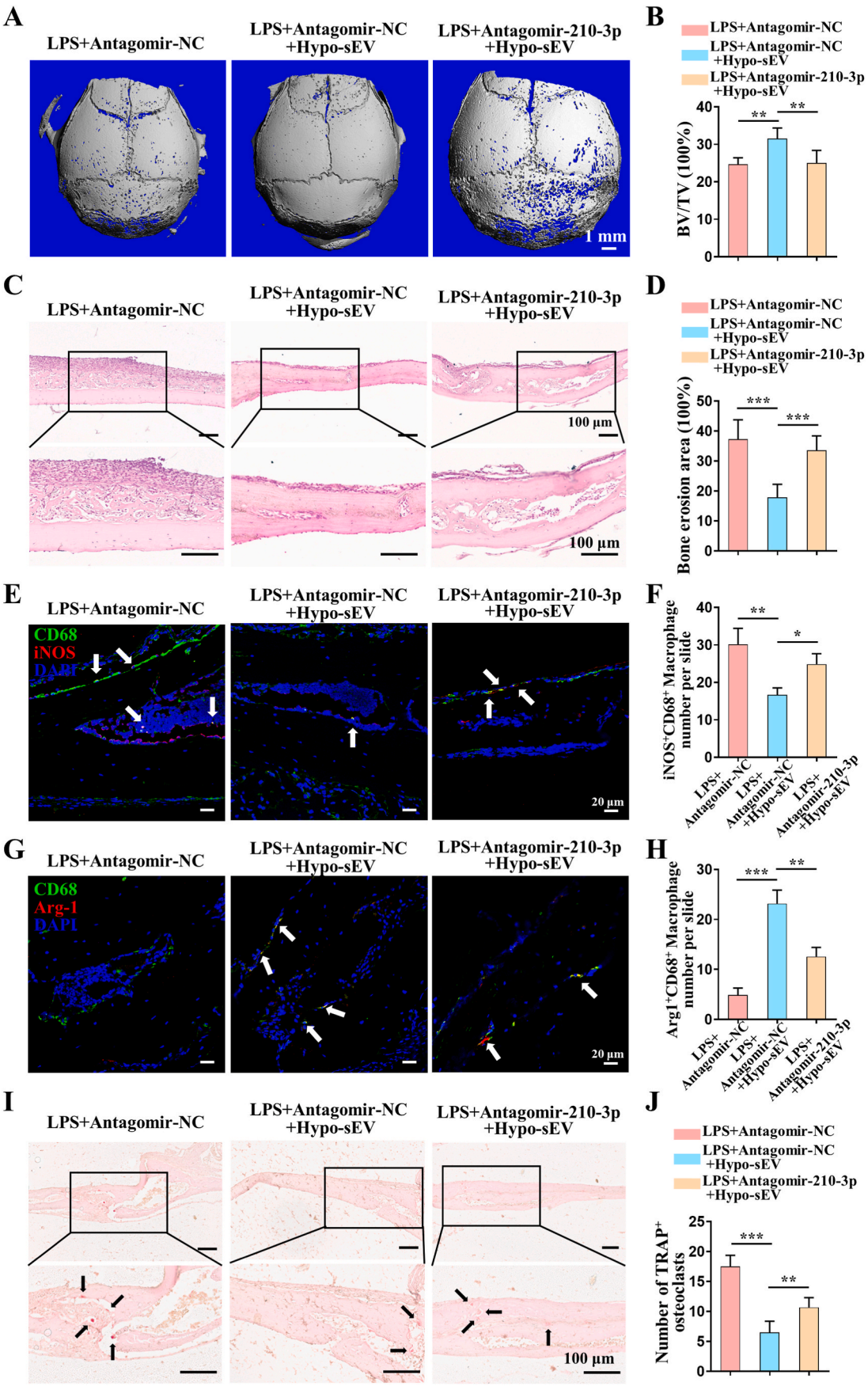

(caption on next page)

Fig. 7. Antagomir-210-3p abrogates the therapeutic effects of Hypo-sEV on LPS-induced inflammatory calvarial bone loss *in vivo*. (A) Micro-CT scanning and subsequent 3D reconstruction of the calvarial bone after the injection of LPS with Hypo-sEV and antagomir-210-3p (n = 5). **(B)** The BV/TV (bone volume/total volume) was analyzed. **(C)** H&E staining showing calvarial destruction and inflammatory cell infiltration. **(D)** The percentage of the bone erosion area in the calvarial bone matrix was determined. **(E)** $CD68^+iNOS^+$ macrophages in the calvarial bone matrix were observed using a laser-scanning confocal microscope (white arrow). **(F)** Statistical analysis of the number of $CD68^+iNOS^+$ macrophages. **(G)** $CD68^+Arg1^+$ macrophages in the calvarial bone matrix were observed using a laser-scanning confocal microscope (white arrow). **(H)** Statistical analysis of the number of $CD68^+Arg1^+$ macrophages. **(I)** Osteoclasts in the calvarial bone matrix after treatment with LPS and Hypo-sEV and antagomir-210-3p were visualized using TRAP staining (dark arrow). **(J)** The histogram shows the number of $TRAP^+$ osteoclasts in the calvarial bone matrix. Error bars represent the mean ± s.d. $^{***}P < 0.005$; $^{**}P < 0.01$; $^{*}P < 0.05$.

RAW264.7 cells. Moreover, miR-210-3p inhibitor treatment abrogated the inhibitory effects of Hypo-sEV on p105 and p50 expression (Fig. 8C and D). Conversely, the miR-210-3p mimic downregulated the expression of p105 and p50 in LPS- or RANKL-treated RAW264.7 cells at the protein and mRNA levels (Fig. 8E and F). These experimental data indicate that miR-210-3p within Hypo-sEV inhibited the expression of NF-κB1 p105. Since a putative miR-210-3p binding site was predicted in the 3′UTR region of NF-κB1 (Fig. 8G), we next verified whether miR-210-3p directly targeted the NF-κB1 3′UTR. Both the wild-type (WT) and mutated (MUT) 3′UTR sequences of NF-κB1 were structured based on potential binding sites (Fig. 8G) and cloned into luciferase reporter vectors. The transfection of the miR-210 mimic significantly reduced NF-κB1-WT luciferase activity but had no obvious effect on luciferase activity in the NF-κB1-MUT group (Fig. 8H), indicating that miR-210-3p directly targets the NF-κB1 3′UTR.

We next also verified the potential of NF-κB1 p105 to regulate macrophage polarization and osteoclastogenesis in the present study. The results showed that *NF-κB1* siRNA treatment decreased the expression of *IL-1β*, *IL-6* and *TNF-α* and upregulated the expression of *IL-10* and *Arg*1 in LPS-treated RAW264.7 cells (Figs. S6A–C). Moreover, *NF-κB1* siRNA treatment suppressed osteoclast formation and the expression of *Acp5*, *CTSK*, *c-FOS*, *DC-STAMP* and *Atp6v0d2* in RANKL-treated RAW264.7 cells (Figs. S6D–F). Taken together, these results indicate that miR-210-3p within Hypo-sEV induced M2 macrophage generation and inhibited osteoclast differentiation by targeting *NF-kB1* (Fig. 9).

4. Discussion and conclusion

In the present study, we used LPS to induce inflammatory bone loss in the calvarial bone matrix. LPS is a critical constituent of the cell wall of gram-negative bacteria and has been identified as a critical pathogen or participant in infective or inflammatory bone destruction diseases, including periodontitis, osteomyelitis, RA and septic arthritis [3,41]. LPS initiates the recruitment and activation of immune cells such as macrophages and further induces the production of various proinflammatory cytokines. These proinflammatory cytokines directly promote osteoclastogenesis and bone resorption. Moreover, the inflammatory microenvironment facilitates osteoclast formation by inducing RANKL secretion [1,2]. In our study, LPS injection significantly increased the formation of M1 macrophages and $TRAP^+$ osteoclasts in the calvarial bone matrix, thereby providing a reliable model to investigate the therapeutic potential of DPSC-sEV under normoxic or hypoxic conditions in inflammatory or infective osteolysis.

Recent studies have verified that hypoxic stimulation promotes the therapeutic effects of sEV derived from BMSCs, umbilical cord MSCs, and adipose stem cells on a variety of diseases, such as skin wounds, bone fractures, insufficient vessel growth, myocardial infarction, Alzheimer's disease and spinal cord injury [4,25,42–46]. As an easily obtained dental MSC, DPSCs with higher proliferation rates are considered great alternatives to BMSCs. However, the effects of hypoxia on the therapeutic potential of DPSC-sEV remain largely unknown. Our recent study revealed that hypoxia-induced DPSC-sEV have enhanced angiogenic potential through the enrichment of LOXL2 compared with control DPSC-sEV [26]. Here, we showed that hypoxia promotes the release of sEV from DPSCs, which is in line with recent studies about the effects of hypoxia on the release of exosomes in tumor cells and umbilical cord MSCs [42,47]. The hypoxia-inducible factor 1-alpha (HIF-1α) activation induced by hypoxia was reported to enhance sEV release by upregulating the expression of Rab27a, which controls the secretion of exosomes [48]. Thus, hypoxia-induced release of DPSC-sEV may be associated with HIF-1α activation. Moreover, hypoxia-induced DPSC-sEV exhibited improved efficacy in promoting M2 macrophage polarization compared with Nor-sEV, which was consistent with previous studies focusing on MSC-sEV derived from other tissues. More importantly, our study identifies a previously unknown role of hypoxia in increasing the capacities of DPSC-sEV or MSC-sEV to suppress osteoclast formation and alleviate LPS-induced inflammatory osteolysis. The formation of mature functional osteoclasts comprises multiple steps including the differentiation of osteoclast precursors into mononuclear preosteoclasts, the fusion of mononuclear preosteoclasts to form multinucleated osteoclasts, and the activation or maturation of osteoclasts capable of bone resorption [49]. TRAP (also called Acp5) is regarded as an osteoclast differentiation marker and DC-STAMP is a critical protein responsible for the cell-cell fusion of osteoclasts [50]. CTSK is the principal protease mediating matrix degradation, and Atp6v0d2 is a key component of the osteoclast-specific proton pump mediating extracellular acidification during bone resorption [51]. Since Hypo-sEV significantly downregulated the expression levels of Acp5, DC-STAMP, CTSK and Atp6v0d2 in osteoclasts, Hypo-sEV may inhibit the formation of mature functional osteoclasts from multiple stages, including osteoclast differentiation, fusion, and bone resorption. Therefore, our results suggest that hypoxia-elicited DPSC-sEV may be a new promising candidate to treat inflammatory or infective osteolysis since they can simultaneously target proinflammatory macrophages and osteoclasts. Further investigations are required to determine whether hypoxia promotes the therapeutic effects of MSC-sEV derived from other tissues on inflammatory bone loss.

MSC-sEV generally contain intravesicular miRNAs, which are responsible for MSC-mediated biological functions by altering the gene expression and functions of recipient cells [52,53]. With regard to how hypoxia promotes the therapeutic efficacy of MSC-sEV, recent studies demonstrated that large numbers of specific miRNAs that mediate the treatment of diseases, including miR-21-3p, miR-31-5p, miR-125b, miR-126, miR-216a-5p and miR-486-5p, were enriched in hypoxia-induced MSC-sEV [25,42,44,45,54,55]. In the present study, our results revealed the altered miRNA profiles of hypoxia-elicited DPSC-sEV. The miR-7578 and miR-187-3p were found to be significantly enriched in Hypo-sEV. The miR-7578 was reported to inhibit the release of the proinflammatory cytokines TNF-α and IL-6 by targeting early growth response 1 (Egr1) in LPS-treated macrophages [34]. However, our results showed that miR-7578 mimic treatment induced the expression of IL-1β, IL-6 and TNF-α. The reason for the contrasting findings remains unclear but may be due to different experimental conditions. A previous study showed that miR-187 could negatively regulate TNF-α and IL-6 expression in LPS-stimulated monocytes [56], which is almost consistent with our results. Nevertheless, our study showed that miR-187-3p mimics increased IL-1β expression. The level of miR-210-3p within DPSC-sEV was also significantly increased by hypoxic preconditioning, which was consistent with a previous report about BMSC-sEV [57]. Furthermore, antagomir-210-3p attenuated the protective effects of Hypo-sEV against LPS-induced inflammatory bone loss, indicating the crucial role of miR-210-3p in hypoxia-elicited DPSC-sEV-mediated therapeutic effects.

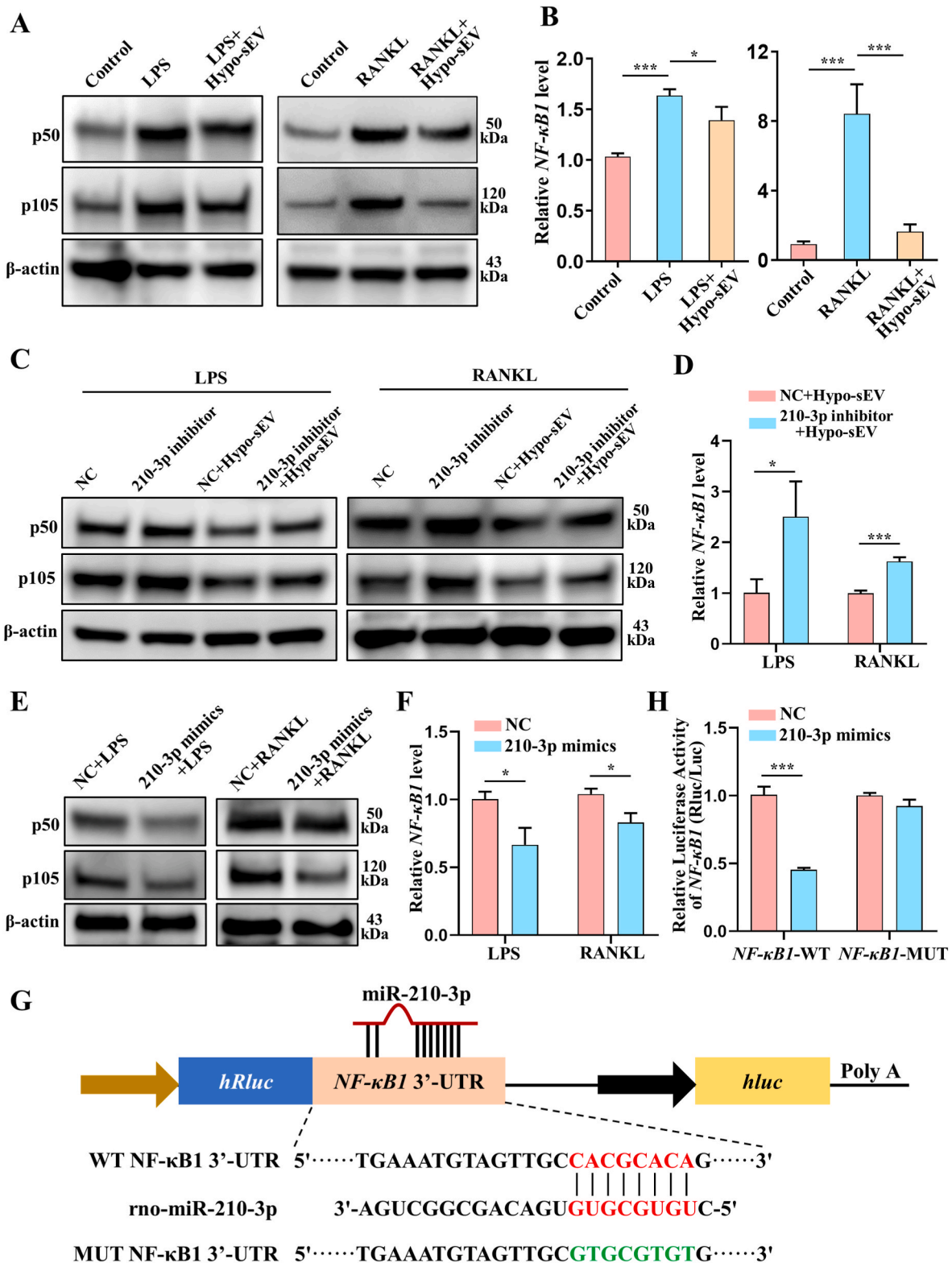

Fig. 8. MiR-210-3p within Hypo-sEV targets *NF-κB1*. (A) The expression of NF-κB1 (p105) and p50 in LPS- or RANKL-treated RAW264.7 cells that were cultured with Hypo-sEV was determined using western blotting. **(B)** qPCR analysis showing the relative mRNA levels of *NF-κB1* in LPS- or RANKL-treated RAW264.7 cells that were cultured with Hypo-sEV. **(C)** The expression of p105 and p50 in LPS- or RANKL-treated RAW264.7 cells that were cultured with Hypo-sEV and the miR-210-3p inhibitor was determined using western blotting. **(D)** qPCR analysis showing the relative mRNA levels of *NF-κB1* in LPS- or RANKL-treated RAW264.7 cells that were cultured with Hypo-sEV and the miR-210-3p inhibitor. **(E)** The expression of p105 and p50 in LPS- or RANKL-treated RAW264.7 cells that were cultured with miR-210-3p mimics was determined using western blotting. **(F)** qPCR analysis showing the relative mRNA levels of *NF-κB1* in LPS- or RANKL-treated RAW264.7 cells that were cultured with miR-210-3p mimics. **(G)** The binding site between miR-210-3p and NF-κB1. **(H)** A luciferase reporter assay was performed to confirm whether NF-κB1 was the target gene of miR-210-3p. Error bars represent the mean ± s.d. $^{***}P < 0.005$; $^{*}P < 0.05$.

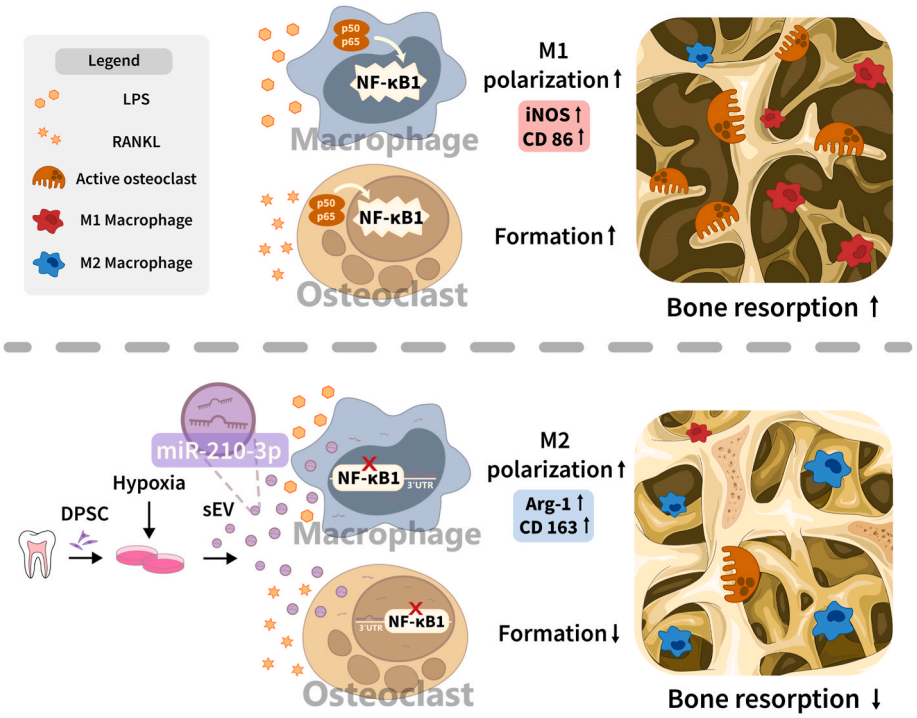

Fig. 9. Schematic diagram showing how miR-210-3p in hypoxia-elicited DPSC-sEV inhibits LPS-induced inflammatory bone loss by targeting *NF-kB1* in macrophages and osteoclasts.

MiR-210 is evolutionarily conserved and ubiquitously expressed in hypoxic cells [58]. Thus, miR-210 is a signature of hypoxia and is known as "a unique and pleiotropic hypoxamir" [59]. The biological effects of miR-210 on immune cells have received extensive attention. It has been reported that hypoxia-inducible factor 1-alpha (HIF-1α) is activated by hypoxia and can directly induce the expression of miR-210, which in turn targets HIF-1α to inhibit the Th17-cell-mediated inflammatory response in experimental colitis [60]. MiR-210 can also be induced by the LPS/TLR4 signaling pathway and functions as a negative regulator of LPS-induced expression of proinflammatory cytokines by targeting NF-κB in macrophages [38]. In addition, miR-210-3p attenuated lipid uptake and inflammatory cytokine production in oxidized low-density lipoprotein (ox-LDL)-exposed macrophages, resulting in protective effects against atherosclerosis [61]. Similarly, we found that Hypo-sEV-stimulated RAW264.7 cells treated with LPS exhibited upregulated levels of miR-210-3p, which plays a critical role in inducing macrophages to acquire an anti-inflammatory phenotype and inhibiting LPS-induced osteolysis. Upon blockage of miR-210-3p, Hypo--sEV-mediated induction of M2 macrophage polarization declined. Conversely, miR-210-3p mimic-treated macrophages showed decreased M1 marker expression and elevated M2 marker expression. Therefore, our study and previous studies suggest that miR-210 may be an important regulator that limits proinflammatory cytokine production and immunopathology. However, previous findings on the effects of miR-210 on inflammatory responses seem controversial. Recent studies have shown that miR-210 induction in activated macrophages supports a switch toward a proinflammatory state by reducing mitochondrial oxidative phosphorylation in favor of glycolysis. Knockout of miR-210 in macrophages protected against sepsis [62]. Furthermore, miR-210-3p expression in plasma EVs were elevated in sepsis and targeted ATG7 to promote sepsis-induced acute lung injury by inhibiting autophagy and activating inflammation in THP-1 macrophages [63]. The reason for these contrasting findings may lie in the different cells or contexts/diseases.

In addition to its immunomodulatory effects, miR-210-3p has also been shown to exert beneficial functions to alleviate cardiovascular disease and promote osteogenesis. MiR-210 could induce neovascularization by regulating SOCS1-STAT3-VEGF-C signaling in mice with cerebral ischemia/reperfusion [64]. MiR-210 in hypoxia-elicited BMSC-sEV inhibited cardiomyocyte apoptosis induced by hypoxia, leading to improved heart function in mice with myocardial infarction [57]. Moreover, miR-210 promoted osteoblastic differentiation of umbilical cord MSCs and bone marrow-derived ST2 stromal cells [65,66]. Since the induction of angiogenesis and osteogenic differentiation in BMSCs is critical for bone repair, it may be worth investigating whether Hypo-sEV can induce angiogenesis and osteogenesis by transferring miR-210-3p during inflammatory osteolysis. Here, we observed that the level of miR-210-3p was increased in RANKL-stimulated RAW264.7 cells after Hypo-sEV treatment. Using the miR-210-3p inhibitor or antagomir-210-3p abrogated the inhibitory effects on osteoclast formation and LPS-induced osteolysis. Conversely, the miR-210-3p mimic inhibited osteoclast differentiation in RANKL-treated RAW264.7 cells. Thus, we identified a novel role of miR-210-3p in inhibiting osteoclastogenesis and bone resorption.

The transcription factor NF-κB plays a crucial role in the inflammatory response and osteoclast formation [67,68]. LPS and RANKL can activate NF-κB signaling by binding with TLR4 or RANK on monocytes/macrophages, respectively, leading to the transcription of large numbers of proinflammatory and osteoclast-related genes, thus inducing M1 macrophage polarization or bone-resorbing osteoclast formation [32,40,69]. Inhibiting NF-κB therefore has been considered an effective approach to inhibit proinflammatory cytokine production in macrophages, as well as osteoclast formation and bone resorptive activity [70,71]. In our study, Hypo-sEV suppressed the expression of NF-κB1/p105, a key functional subunit of NF-κB, to induce M2 macrophage polarization and inhibit osteoclastogenesis. p105, a precursor of p50, can be processed into mature p50, which forms dimers with p65 (also named RelA). The p65/p50 heterodimer is the most common form of the NF-κB dimer and can bind to the DNA consensus sequences of various target genes after translocation to the nucleus [72,73]. Our results demonstrated that the transfection of miR-210-3p inhibitors into LPS- or RANKL-treated RAW264.7 cells partially interfered with the ability of

Hypo-sEV to inhibit p105/p50 expression, suggesting that Hypo-sEV attenuated the expression of p105/p50 by transferring miR-210-3p. In contrast, miR-210-3p mimics significantly inhibited p105/p50 protein expression induced by LPS or RANKL in RAW264.7 cells. More importantly, transfection of the miR-210-3p mimics markedly suppressed the activation of the luciferase reporter with the NF-κB1 3′UTR. Thus, our data identified the dual roles of miR-210-3p in simultaneously inducing M2 macrophage polarization and inhibiting osteoclastogenesis by targeting NF-κB1.

In summary, our results reveal that hypoxia preconditioning not only induced the secretion of DPSC-sEV, but also enhanced the DPSC-sEV-mediated therapeutic effect on LPS-induced osteolysis. The enrichment of miR-210-3p in Hypo-sEV contributes to protecting bone by simultaneously inducing M2 macrophage polarization and inhibiting osteoclastogenesis by targeting NF-κB1. This “two birds, one stone” (two target cells, one sEV or miRNA) effect of hypoxia-induced DPSC-sEV or miR-210-3p may present a promising approach for developing strategies to treat inflammatory or infective osteolysis (Fig. 9). Since osteomyelitis, periodontitis, peri-implantitis, RA and septic arthritis are common conditions associated with inflammatory or infective osteolysis, further investigations are required to verify the therapeutic effects of hypoxia-induced DPSC-sEV in these diseases.

CRediT authorship contribution statement

Jun Tian: Conceptualization, Methodology, Writing – original draft. **Weiyang Chen:** Methodology, Writing – original draft, Software. **Yuhua Xiong:** Methodology, Validation, Software. **Qianer Li:** Investigation, Methodology. **Siyi Kong:** Methodology. **Mengjie Li:** Resources, Formal analysis, Validation. **Chunfeng Pang:** Formal analysis, Investigation. **Yu Qiu:** Resources. **Zhezhen Xu:** Formal analysis, Funding acquisition. **Qimei Gong:** Conceptualization, Writing – review & editing, Funding acquisition. **Xi Wei:** Supervision, Conceptualization, Writing – review & editing, Funding acquisition.

Declaration of competing interest

The authors declare that they have no known competing financial interests or personal relationships that could have appeared to influence the work reported in this paper.

Acknowledgements

This work was supported by National Natural Science Foundation of China (No. 81870750, 81970925, 81900994) and the Guangdong Financial Fund for High-Caliber Hospital Construction (174-2018-XMZC-0001-03-0125/D-08).

Appendix A. Supplementary data

Supplementary data to this article can be found online at https://doi.org/10.1016/j.bioactmat.2022.10.001.

References

[1] H. Wu, B. Hu, X. Zhou, C. Zhou, J. Meng, Y. Yang, X. Zhao, Z. Shi, S. Yan, Artemether attenuates LPS-induced inflammatory bone loss by inhibiting osteoclastogenesis and bone resorption via suppression of MAPK signaling pathway, Cell Death Dis. 9 (2018) 498.
[2] A. Kassem, P. Henning, P. Lundberg, P.P. Souza, C. Lindholm, U.H. Lerner, Porphyromonas gingivalis stimulates bone resorption by enhancing RANKL (receptor activator of NF-κB ligand) through activation of toll-like receptor 2 in osteoblasts, J. Biol. Chem. 290 (2015) 20147–20158.
[3] S.C. Kwak, J.M. Baek, C.H. Lee, K.H. Yoon, M.S. Lee, J.Y. Kim, Umbelliferone prevents lipopolysaccharide-induced bone loss and suppresses RANKL-induced osteoclastogenesis by attenuating Akt-c-Fos-NFATc1 signaling, Int. J. Biol. Sci. 15 (2019) 2427–2437.
[4] Y. Niu, Z. Wang, Y. Shi, L. Dong, C. Wang, Modulating macrophage activities to promote endogenous bone regeneration: biological mechanisms and engineering approaches, Bioact. Mater. 6 (2021) 244–261.
[5] S.S. Li, S.H. He, P.Y. Xie, W. Li, X.X. Zhang, T.F. Li, D.F. Li, Recent progresses in the treatment of osteoporosis, Front. Pharmacol. 12 (2021), 717065.
[6] Y. Han, J. Yang, J. Fang, Y. Zhou, E. Candi, J. Wang, D. Hua, C. Shao, Y. Shi, The secretion profile of mesenchymal stem cells and potential applications in treating human diseases, Signal Transduct. Targeted Ther. 7 (2022) 92.
[7] J. Tian, X. Kou, R. Wang, H. Jing, C. Chen, J. Tang, X. Mao, B. Zhao, X. Wei, S. Shi, Autophagy controls mesenchymal stem cell therapy in psychological stress colitis mice, Autophagy 17 (2021) 2586-2603.
[8] M. Nie, B. Kong, G. Chen, Y. Xie, Y. Zhao, L. Sun, MSCs-laden injectable self-healing hydrogel for systemic sclerosis treatment, Bioact. Mater. 17 (2022) 369–378.
[9] C.R. Harrell, N. Jovicic, V. Djonov, N. Arsenijevic, V. Volarevic, Mesenchymal stem cell-derived exosomes and other extracellular vesicles as new remedies in the therapy of inflammatory diseases, Cells 8 (2019) 1065.
[10] X. Xiao, M. Xu, H. Yu, L. Wang, X. Li, J. Rak, S. Wang, R.C. Zhao, Mesenchymal stem cell-derived small extracellular vesicles mitigate oxidative stress-induced senescence in endothelial cells via regulation of miR-146a/Src, Signal Transduct. Targeted Ther. 6 (2021) 354.
[11] K.S. Lee, J. Lee, H.K. Kim, S.H. Yeom, C.H. Woo, Y.J. Jung, Y.E. Yun, S.Y. Park, J. Han, E. Kim, J.H. Sul, J.M. Jung, J.H. Park, J.S. Choi, Y.W. Cho, D.G. Jo, Extracellular vesicles from adipose tissue-derived stem cells alleviate osteoporosis through osteoprotegerin and miR-21-5p, J. Extracell. Vesicles 10 (2021), e12152.
[12] Q. Wu, X. Fu, X. Li, J. Li, W. Han, Y. Wang, Modification of adipose mesenchymal stem cells-derived small extracellular vesicles with fibrin-targeting peptide CREKA for enhanced bone repair, Bioact. Mater. 20 (2023) 208–220.
[13] M. Kang, C.C. Huang, P. Gajendrareddy, Y. Lu, S. Shirazi, S. Ravindran, L. F. Cooper, Extracellular vesicles from TNFα preconditioned MSCs: effects on immunomodulation and bone regeneration, Front. Immunol. 13 (2022), 878194.
[14] D.G. You, G.T. Lim, S. Kwon, W. Um, B.H. Oh, S.H. Song, J. Lee, D.G. Jo, Y.W. Cho, J.H. Park, Metabolically engineered stem cell-derived exosomes to regulate macrophage heterogeneity in rheumatoid arthritis, Sci. Adv. 7 (2021), eabe0083.
[15] Z. Shen, S. Kuang, Y. Zhang, M. Yang, W. Qin, X. Shi, Z. Lin, Chitosan hydrogel incorporated with dental pulp stem cell-derived exosomes alleviates periodontitis in mice via a macrophage-dependent mechanism, Bioact. Mater. 5 (2020) 1113–1126.
[16] Y. Nakao, T. Fukuda, Q. Zhang, T. Sanui, T. Shinjo, X. Kou, C. Chen, D. Liu, Y. Watanabe, C. Hayashi, H. Yamato, K. Yotsumoto, U. Tanaka, T. Taketomi, T. Uchiumi, A.D. Le, S. Shi, F. Nishimura, Exosomes from TNF-α-treated human gingiva-derived MSCs enhance M2 macrophage polarization and inhibit periodontal bone loss, Acta Biomater. 122 (2021) 306–324.
[17] F. Xiao, B. Zuo, B. Tao, C. Wang, Y. Li, J. Peng, C. Shen, Y. Cui, J. Zhu, X. Chen, Exosomes derived from cyclic mechanical stretch-exposed bone marrow mesenchymal stem cells inhibit RANKL-induced osteoclastogenesis through the NF-κB signaling pathway, Ann. Transl. Med. 9 (2021) 798.
[18] C. Liu, F. Hu, G. Jiao, Y. Guo, P. Zhou, Y. Zhang, Z. Zhang, J. Yi, Y. You, Z. Li, H. Wang, X. Zhang, Dental pulp stem cell-derived exosomes suppress M1 macrophage polarization through the ROS-MAPK-NFκB P65 signaling pathway after spinal cord injury, J. Nanobiotechnol. 20 (2022) 65.
[19] S. Gronthos, M. Mankani, J. Brahim, P.G. Robey, S. Shi, Postnatal human dental pulp stem cells (DPSCs) *in vitro* and *in vivo*, Proc. Natl. Acad. Sci. U.S.A. 97 (2000) 13625–13630.
[20] L. Ji, L. Bao, Z. Gu, Q. Zhou, Y. Liang, Y. Zheng, Y. Xu, X. Zhang, X. Feng, Comparison of immunomodulatory properties of exosomes derived from bone marrow mesenchymal stem cells and dental pulp stem cells, Immunol. Res. 67 (2019) 432–442.
[21] H. Zhou, X. Li, Y. Yin, X.T. He, Y. An, B.M. Tian, Y.L. Hong, L.A. Wu, F.M. Chen, The proangiogenic effects of extracellular vesicles secreted by dental pulp stem cells derived from periodontally compromised teeth, Stem Cell Res. Ther. 11 (2020) 110.
[22] Y. Li, X. Duan, Y. Chen, B. Liu, G. Chen, Dental stem cell-derived extracellular vesicles as promising therapeutic agents in the treatment of diseases, Int. J. Oral Sci. 14 (2022) 2.
[23] Q. Jin, P. Li, K. Yuan, F. Zhao, X. Zhu, P. Zhang, Z. Huang, Extracellular vesicles derived from human dental pulp stem cells promote osteogenesis of adipose-derived stem cells via the MAPK pathway, J. Tissue Eng. 11 (2020), 2041731420975569.
[24] Y. Imanishi, M. Hata, R. Matsukawa, A. Aoyagi, M. Omi, M. Mizutani, K. Naruse, S. Ozawa, M. Honda, T. Matsubara, J. Takebe, Efficacy of extracellular vesicles from dental pulp stem cells for bone regeneration in rat calvarial bone defects, Inflamm. Regen. 41 (2021) 12.
[25] W. Liu, Y. Rong, J. Wang, Z. Zhou, X. Ge, C. Ji, D. Jiang, F. Gong, L. Li, J. Chen, S. Zhao, F. Kong, C. Gu, J. Fan, W. Cai, Exosome-shuttled miR-216a-5p from hypoxic preconditioned mesenchymal stem cells repair traumatic spinal cord injury by shifting microglial M1/M2 polarization, J. Neuroinflammation 17 (2020) 47.
[26] B. Li, X. Xian, X. Lin, L. Huang, A. Liang, H. Jiang, Q. Gong, Hypoxia alters the proteome profile and enhances the angiogenic potential of dental pulp stem cell-derived exosomes, Biomolecules 12 (2022) 575.
[27] X. Wu, K. Zhao, X. Fang, F. Lu, W. Zhang, X. Song, L. Chen, J. Sun, H. Chen, Inhibition of lipopolysaccharide-induced inflammatory bone loss by Saikosaponin D is associated with regulation of the RANKL/RANK pathway, Drug Des. Dev. Ther. 15 (2021) 4741–4757.
[28] Z. Zhuang, S. Yoshizawa-Smith, A. Glowacki, K. Maltos, C. Pacheco, M. Shehabeldin, M. Mulkeen, N. Myers, R. Chong, K. Verdelis, G.P. Garlet, S. Little,

C. Sfeir, Induction of M2 macrophages prevents bone loss in murine periodontitis models, J. Dent. Res. 98 (2019) 200–208.
[29] Y.H. Kim, R.O.C. Oreffo, J.I. Dawson, From hurdle to springboard: the macrophage as target in biomaterial-based bone regeneration strategies, Bone 159 (2022), 116389.
[30] P. Zhou, D. Xia, Z. Ni, T. Ou, Y. Wang, H. Zhang, L. Mao, K. Lin, S. Xu, J. Liu, Calcium silicate bioactive ceramics induce osteogenesis through oncostatin M, Bioact. Mater. 6 (2021) 810–822.
[31] K. Redlich, J.S. Smolen, Inflammatory bone loss: pathogenesis and therapeutic intervention, Nat. Rev. Drug Discov. 11 (2012) 234–250.
[32] X. Wang, Y. Yu, L. Ji, Z. Geng, J. Wang, C. Liu, Calcium phosphate-based materials regulate osteoclast-mediated osseointegration, Bioact. Mater. 6 (2021) 4517–4530.
[33] X. Ji, L. Yang, Z. Zhang, K. Zhang, N. Chang, X. Zhou, L. Hou, L. Yang, L. Li, Sphingosine 1-phosphate/microRNA-1249-5p/MCP-1 axis is involved in macrophage-associated inflammation in fatty liver injury in mice, Eur. J. Immunol. 50 (2020) 1746–1756.
[34] J. Zhang, S. Xie, W. Ma, Y. Teng, Y. Tian, X. Huang, Y. Zhang, A newly identified microRNA, mmu-miR-7578, functions as a negative regulator on inflammatory cytokines tumor necrosis factor-α and interleukin-6 via targeting Egr1 in vivo, J. Biol. Chem. 288 (2013) 4310–4320.
[35] Y. Xu, X. Tang, A. Fang, J. Yan, D. Kofi Wiredu Ocansey, X. Zhang, F. Mao, HucMSC-Ex carrying miR-203a-3p.2 ameliorates colitis through the suppression of caspase11/4-induced macrophage pyroptosis, Int. Immunopharm. 110 (2022), 108925.
[36] G. Curtale, M. Rubino, M. Locati, MicroRNAs as molecular switches in macrophage activation, Front. Immunol. 10 (2019) 799.
[37] K. Essandoh, Y. Li, J. Huo, G.C. Fan, MiRNA-mediated macrophage polarization and its potential role in the regulation of inflammatory response, Shock 46 (2016) 122–131.
[38] J. Qi, Y. Qiao, P. Wang, S. Li, W. Zhao, C. Gao, microRNA-210 negatively regulates LPS-induced production of proinflammatory cytokines by targeting NF-κB1 in murine macrophages, FEBS Lett. 586 (2012) 1201–1207.
[39] D.V. Novack, Role of NF-κB in the skeleton, Cell Res. 21 (2011) 169–182.
[40] T. Liu, L. Zhang, D. Joo, S.C. Sun, NF-κB signaling in inflammation, Signal Transduct. Targeted Ther. 2 (2017), 17023.
[41] M. Li, J. Tian, Z. Xu, Q. Zeng, W. Chen, S. Lei, X. Wei, Histology-based profile of inflammatory mediators in experimentally induced pulpitis in a rat model: screening for possible biomarkers, Int. Endod. J. 54 (2021) 1328–1341.
[42] W. Liu, L. Li, Y. Rong, D. Qian, J. Chen, Z. Zhou, Y. Luo, D. Jiang, L. Cheng, S. Zhao, F. Kong, J. Wang, Z. Zhou, T. Xu, F. Gong, Y. Huang, C. Gu, X. Zhao, J. Bai, F. Wang, W. Zhao, L. Zhang, X. Li, G. Yin, J. Fan, W. Cai, Hypoxic mesenchymal stem cell-derived exosomes promote bone fracture healing by the transfer of miR-126, Acta Biomater. 103 (2020) 196–212.
[43] H. Gonzalez-King, N.A. García, I. Ontoria-Oviedo, M. Ciria, J.A. Montero, P. Sepúlveda, Hypoxia inducible factor-1α potentiates jagged 1-mediated angiogenesis by mesenchymal stem cell-derived exosomes, Stem Cell. 35 (2017) 1747–1759.
[44] L.P. Zhu, T. Tian, J.Y. Wang, J.N. He, T. Chen, M. Pan, L. Xu, H.X. Zhang, X.T. Qiu, C.C. Li, K.K. Wang, H. Shen, G.G. Zhang, Y.P. Bai, Hypoxia-elicited mesenchymal stem cell-derived exosomes facilitates cardiac repair through miR-125b-mediated prevention of cell death in myocardial infarction, Theranostics 8 (2018) 6163–6177.
[45] Q. Li, Y. Xu, K. Lv, Y. Wang, Z. Zhong, C. Xiao, K. Zhu, C. Ni, K. Wang, M. Kong, X. Li, Y. Fan, F. Zhang, Q. Chen, Y. Li, Q. Li, C. Liu, J. Zhu, S. Zhong, J. Wang, Y. Chen, J. Zhao, D. Zhu, R. Wu, J. Chen, W. Zhu, H. Yu, R. Ardehali, J.J. Zhang, J. Wang, X. Hu, Small extracellular vesicles containing miR-486-5p promote angiogenesis after myocardial infarction in mice and nonhuman primates, Sci. Transl. Med. 13 (2021), eabb0202.
[46] S. Chen, F. Sun, H. Qian, W. Xu, J. Jiang, Preconditioning and engineering strategies for improving the efficacy of mesenchymal stem cell-derived exosomes in cell-free therapy, Stem Cell. Int. 2022 (2022), 1779346.
[47] C. Shao, F. Yang, S. Miao, W. Liu, C. Wang, Y. Shu, H. Shen, Role of hypoxia-induced exosomes in tumor biology, Mol. Cancer 17 (2018) 120.
[48] K.D.P. Dorayappan, R. Wanner, J.J. Wallbillich, U. Saini, R. Zingarelli, A.A. Suarez, D.E. Cohn, K. Selvendiran, Hypoxia-induced exosomes contribute to a more aggressive and chemoresistant ovarian cancer phenotype: a novel mechanism linking STAT3/Rab proteins, Oncogene 37 (2018) 3806–3821.
[49] J. Tian, W. Qi, Y. Zhang, M. Glogauer, Y. Wang, Z. Lai, H. Jiang, Bioaggregate inhibits osteoclast differentiation, fusion, and bone resorption in vitro, J. Endod. 41 (2015) 1500–1506.
[50] M. Yagi, T. Miyamoto, Y. Sawatani, K. Iwamoto, N. Hosogane, N. Fujita, K. Morita, K. Ninomiya, T. Suzuki, K. Miyamoto, Y. Oike, M. Takeya, Y. Toyama, T. Suda, DC-STAMP is essential for cell–cell fusion in osteoclasts and foreign body giant cells, J. Exp. Med. 202 (2005) 345–351.
[51] H. Wu, G. Xu, Y.P. Li, Atp6v0d2 is an essential component of the osteoclast-specific proton pump that mediates extracellular acidification in bone resorption, J. Bone Miner. Res. 24 (2009) 871–885.
[52] K.W. Witwer, B.W.M. Van Balkom, S. Bruno, A. Choo, M. Dominici, M. Gimona, A. F. Hill, D. De Kleijn, M. Koh, R.C. Lai, S.A. Mitsialis, L.A. Ortiz, E. Rohde, T. Asada, W.S. Toh, D.J. Weiss, L. Zheng, B. Giebel, S.K. Lim, Defining mesenchymal stromal cell (MSC)-derived small extracellular vesicles for therapeutic applications, J. Extracell. Vesicles 8 (2019), 1609206.
[53] B. Liu, Y. Kong, W. Shi, M. Kuss, K. Liao, G. Hu, P. Xiao, J. Sankarasubramanian, C. Guda, X. Wang, Y. Lei, B. Duan, Exosomes derived from differentiated human ADMSC with the Schwann cell phenotype modulate peripheral nerve-related cellular functions, Bioact. Mater. 14 (2022) 61–75.
[54] J. Wang, H. Wu, Y. Peng, Y. Zhao, Y. Qin, Y. Zhang, Z. Xiao, Hypoxia adipose stem cell-derived exosomes promote high-quality healing of diabetic wound involves activation of PI3K/Akt pathways, J. Nanobiotechnol. 19 (2021) 202.
[55] X.F. Zhang, T. Wang, Z.X. Wang, K.P. Huang, Y.W. Zhang, G.L. Wang, H.J. Zhang, Z.H. Chen, C.Y. Wang, J.X. Zhang, H. Wang, Hypoxic ucMSC-secreted exosomal miR-125b promotes endothelial cell survival and migration during wound healing by targeting TP53INP1, Mol. Ther. Nucleic Acids 26 (2021) 347–359.
[56] M. Rossato, G. Curtale, N. Tamassia, M. Castellucci, L. Mori, S. Gasperini, B. Mariotti, M. De Luca, M. Mirolo, M.A. Cassatella, M. Locati, F. Bazzoni, IL-10-induced microRNA-187 negatively regulates TNF-α, IL-6, and IL-12p40 production in TLR4-stimulated monocytes, Proc. Natl. Acad. Sci. U.S.A. 109 (2012) E3101–E3110.
[57] H. Cheng, S. Chang, R. Xu, L. Chen, X. Song, J. Wu, J. Qian, Y. Zou, J. Ma, Hypoxia-challenged MSC-derived exosomes deliver miR-210 to attenuate post-infarction cardiac apoptosis, Stem Cell Res. Ther. 11 (2020) 224.
[58] S.Y. Chan, J. Loscalzo, MicroRNA-210: a unique and pleiotropic hypoxamir, Cell Cycle 9 (2010) 1072–1083.
[59] X.Q. Hu, C. Dasgupta, R. Song, M. Romero, S.M. Wilson, L. Zhang, MicroRNA-210 mediates hypoxia-induced repression of spontaneous transient outward currents in sheep uterine arteries during gestation, Hypertension 77 (2021) 1412–1427.
[60] H. Wang, H. Flach, M. Onizawa, L. Wei, M.T. McManus, A. Weiss, Negative regulation of Hif1a expression and TH17 differentiation by the hypoxia-regulated microRNA miR-210, Nat. Immunol. 15 (2014) 393–401.
[61] X.R. Qiao, L. Wang, M. Liu, Y. Tian, T. Chen, MiR-210-3p attenuates lipid accumulation and inflammation in atherosclerosis by repressing IGF2, Biosci, Biotechnol., Biochem. 84 (2020) 321–329.
[62] F. Virga, F. Cappellesso, B. Stijlemans, A.T. Henze, R. Trotta, J. Van Audenaerde, A. S. Mirchandani, M.A. Sanchez-Garcia, J. Vandewalle, F. Orso, C. Riera-Domingo, A. Griffa, C. Ivan, E. Smits, D. Laoui, F. Martelli, L. Langouche, G. Van den Berghe, O. Feron, B. Ghesquière, H. Prenen, C. Libert, S.R. Walmsley, C. Corbet, J.A. Van Ginderachter, M. Ivan, D. Taverna, M. Mazzone, Macrophage miR-210 induction and metabolic reprogramming in response to pathogen interaction boost life-threatening inflammation, Sci. Adv. 7 (2021), eabf0466.
[63] G. Li, B. Wang, X. Ding, X. Zhang, J. Tang, H. Lin, Plasma extracellular vesicle delivery of miR-210-3p by targeting ATG7 to promote sepsis-induced acute lung injury by regulating autophagy and activating inflammation, Exp. Mol. Med. 53 (2021) 1180–1191.
[64] Z.Y. Meng, H.L. Kang, W. Duan, J. Zheng, Q.N. Li, Z.J. Zhou, MicroRNA-210 promotes accumulation of neural precursor cells around ischemic Foci after cerebral ischemia by regulating the SOCS1-STAT3-VEGF-C pathway, J. Am. Heart Assoc. 7 (2018), e005052.
[65] A. Asgharzadeh, S. Alizadeh, M.R. Keramati, M. Soleimani, A. Atashi, M. Edalati, Z. Kashani Khatib, M. Rafiee, M. Barzegar, H. Razavi, Upregulation of miR-210 promotes differentiation of mesenchymal stem cells (MSCs) into osteoblasts, Bosn. J. Basic Med. Sci. 18 (2018) 328–335.
[66] Y. Mizuno, Y. Tokuzawa, Y. Ninomiya, K. Yagi, Y. Yatsuka-Kanesaki, T. Suda, T. Fukuda, T. Katagiri, Y. Kondoh, T. Amemiya, H. Tashiro, Y. Okazaki, miR-210 promotes osteoblastic differentiation through inhibition of AcvR1b, FEBS Lett. 583 (2009) 2263–2268.
[67] J. Chang, Z. Wang, E. Tang, Z. Fan, L. McCauley, R. Franceschi, K. Guan, P. H. Krebsbach, C.Y. Wang, Inhibition of osteoblastic bone formation by nuclear factor-kappaB, Nat. Med. 15 (2009) 682–689.
[68] V. Iotsova, J. Caamaño, J. Loy, Y. Yang, A. Lewin, R. Bravo, Osteopetrosis in mice lacking NF-kappaB1 and NF-kappaB2, Nat. Med. 3 (1997) 1285–1289.
[69] Y. Wang, X. Ren, W. Li, R. Cao, S. Liu, L. Jiang, B. Cheng, J. Xia, SPDEF suppresses head and neck squamous cell carcinoma progression by transcriptionally activating NR4A1, Int. J. Oral Sci. 13 (2021) 33.
[70] H.S. Son, J. Lee, H.I. Lee, N. Kim, Y.J. Jo, G.R. Lee, S.E. Hong, M. Kwon, N.Y. Kim, H.J. Kim, J.H. Park, S.Y. Lee, W. Jeong, Benzydamine inhibits osteoclast differentiation and bone resorption via down-regulation of interleukin-1 β expression, Acta Pharm. Sin. B 10 (2020) 462–474.
[71] X. Zhou, Z. Zhang, W. Jiang, M. Hu, Y. Meng, W. Li, X. Zhou, C. Wang, Naringenin is a potential anabolic treatment for bone loss by modulating osteogenesis, osteoclastogenesis, and macrophage polarization, Front. Pharmacol. 13 (2022), 872188.
[72] C.M. Fan, T. Maniatis, Generation of p50 subunit of NF-kappa B by processing of p105 through an ATP-dependent pathway, Nature 354 (1991) 395–398.
[73] C. Acta BiomaterGiuliani, I. Bucci, G. Napolitano, The role of the transcription factor nuclear factor-kappa B in thyroid autoimmunity and cancer, Front. Endocrinol. 9 (2018) 471.